UNIVERSIDADE FEDERAL DE SANTA CATARINA - UFSC
CENTRO DE CIÊNCIAS FÍSICAS E MATEMÁTICAS - CFM
DEPARTAMENTO DE FÍSICA
CURSO DE PÓS-GRADUAÇÃO EM FÍSICA

Tulio Eduardo Restrepo Medina

RADIATIVELY INDUCED VECTOR REPULSION FOR LIGHT QUARKS

Florianópolis
2014

Tulio Eduardo Restrepo Medina

GERAÇÃO RADIATIVA DE REPULSÃO VETORIAL PARA QUARKS LEVES

Dissertação submetida ao Curso de Pós-Graduação em Física para a obtenção do grau de Mestre em Física.

Orientador: Prof. Dr. Marcus Emmanuel Benghi Pinto

Florianópolis
2014

Ficha de identificação da obra elaborada pelo autor,
através do Programa de Geração Automática da Biblioteca Universitária da UFSC.

Medina, Tulio Eduardo
Radiatively Induced Vector Repulsion for Light Quarks
/ Tulio Eduardo Medina ; orientador, Marcus Emmanuel
Benghi Pinto - Florianópolis, SC, 2014.
72 p.

Dissertação (mestrado) - Universidade Federal de Santa
Catarina, Centro de Ciências Físicas e Matemáticas.
Programa de Pós-Graduação em Física.

Inclui referências

1. Física. 2. Teoria quântica de campos. 3. Cromodinâmica
quântica à temperatura finita. I. Benghi Pinto, Marcus
Emmanuel. II. Universidade Federal de Santa Catarina.
Programa de Pós-Graduação em Física. III. Título.

ACKNOWLEDGEMENTS

First of all, I would like to thank my parents for their support in my decisions and for their understanding during my stay here in Brazil.

I would like to thank Rodrigo Rocha, Jose Rocha, Sergio Rocha , Moacir Rocha, Vanderlei Valim and Bianca Vega for making me feel like family and for all the good moments here in Brazil.

Moreover, I would like to thank my supervisor, Marcus Benghi Pinto, for his patience and for teaching me so much in these two years. Big thanks to Camilo Macias and Gabriel Ferrari for all the discussions and help in the investigations carried out in this dissertation.

I would like to express my gratitude to Antonio for all the help and for always being so kind to all the students.

I also gratefully acknowledge the reviewers of this dissertation, Professor Rudnei de Oliveira Ramos, Professor Débora Peres Menezes, Professor Pawel Klimas and Professor Emmanuel Gräve de Oliveira.

Finally, I would like to thank CNPq for the financial support and the physics graduate program of the Universidade Federal de Santa Catarina for giving me the opportunity to study in this great and beautiful country.

Abstract

We apply a non-perturbative analytical method, known as the Optimized Perturbation Theory (OPT), to the Polyakov–Nambu–Jona-Lasinio (PNJL) model in order to investigate physical quantities associated with the QCD phase transitions. We consider the Taylor expansion of the pressure in powers of μ/T obtaining the second cumulant (c_2) which is associated to the quark number susceptibility. We discuss how the OPT finite N_c radiative (quantum) corrections induce a contribution to the pressure which behaves as a vector repulsion even when such a channel is absent in the original classical potential. Our results are then compared with the ones furnished by lattice QCD simulations and by the large-N_c approximation showing that, physically, the OPT results resemble those furnished by the latter approximation when a repulsive vector channel is explicitly included in the classical potential. In this case, both approximations fail to correctly describe the Stefan-Boltzmann limit at high temperatures. We discuss how this problem can be circumvented by taking the couplings to be temperature dependent so as to simulate the phenomenon of asymptotic freedom. Since this is the first time the OPT is applied to the PNJL we also discuss many technicalities associated with the evaluation of two loop (exchange) diagrams.

Key words: Optimized Perturbation Theory, Polyakov–Nambu–Jona-Lasinio model, cumulants, susceptibilities, vector channel, lattice QCD, large-N_c approximation, Stefan-Boltzmann limit, chiral symmetry, confinement, non-perturbative methods.

Resumo

Neste trabalho o método analítico não perturbativo conhecido como Teoria de Perturbação Otimizada (OPT) é aplicada ao modelo de Polyakov–Nambu–Jona-Lasinio (PNJL) para que quantidades físicas, associadas com as transições de fase da QCD, possam ser calculadas. A expansão da pressão em potências de μ/T é considerada para obter o segundo cumulante (c_2) que é uma quantidade relacionada com a susceptibilidade do número de quarks. Primeiramente discutimos como as correções radiativas de N_c finito geradas pela OPT produzem uma contribuição que se comporta como um termo vetorial repulsivo mesmo quando este tipo de canal está ausente no potencial clássico original. Em seguida, nossos resultados são comparados com aqueles fornecidos pelas simulações na rede e também pela aproximação de N_c grande (LN). Fisicamente, os resultados da OPT são similares aqueles fornecidos pela aproximação LN quando um canal vetorial repulsivo é explicitamente incluido no potencial clássico. Neste caso, nenhuma destas aproximações analíticas produz corretamente o limite de Stefan Boltzmann para altas temperaturas. Contudo, nossos resultados sugerem como estes problemas podem ser contornados tomando-se as constantes de acoplamento como sendo dependentes da temperatura, de maneira que o fenômeno da liberdade assimptótica possa ser simulado. Esta é a primeira vez que a OPT é aplicada ao modelo de PNJL e por isto vários aspectos técnicos relacionados com o cálculo de diagramas de dois laços são também aqui apresentados.

Palavras chave: Teoria de Perturbação Otimizada, modelo de Polyakov–Nambu–Jona-Lasinio, cumulantes, susceptibilidades, canal vetorial repulsivo, simulações na rede, aproximação de N_c grande, limite de Stefan Boltzmann, simetria quiral, confinamento, métodos não perturbativos.

Contents

List of Figures

List of Tables

1. Introduction

The existence of the universe as we know it, relies on the properties of nuclei and, strictly speaking, on the dynamics of quarks and gluons in quantum chromodynamics (QCD).

In the early universe the matter was in a state of pure quarks and gluons called the quark-gluon plasma (QGP), where density and temperature were extremely high. The relativistic Heavy-Ion Collider (RHIC) discovered the QGP at high temperatures and the Large Hadron Collider (LHC), at CERN, confirmed this discovery at an even higher energies.

It is also believed that the QGP exists in the deep interior of compact stellar objects such as neutron stars where dense QCD matter is realized [1].

Without strong medium effects quarks and gluons are confined inside hadrons and this property is generally called *color confinement*, which is a consequence of the non-perturbative and non-linear dynamics of QCD. Although confinement is a very difficult aspect of QCD, it can be formulated unambiguously in hot QCD with quarks made infinitely heavy. This implies that the order parameter of quark confinement cannot have a strict meaning in the presence of light quarks. At the same time, since gluons have no mass, gluon confinement cannot be given in a simple way.

Quantum electrodynamics (QED) is a perturbative theory, because it has a weak coupling constant ($\alpha = 1/\sqrt{137}$) and perturbation theory is permitted. In contrast, the QCD coupling constant is high at low energies and perturbation theory is not valid. Nevertheless, due to the asymptotic freedom phenomenon, at high energies the coupling is low again. The coupling constant of QCD at one loop order is given by [2]

$$\alpha_s\left(Q^2\right) \equiv \frac{g^2\left(Q^2\right)}{4\pi} = \frac{4\pi}{\left(11 - \frac{2}{3}N_f\right)\ln\left(Q^2/\Lambda^2_{QCD}\right)}, \tag{1.1}$$

where Q^2 is the three-momentum, N_f is the number of flavors and Λ_{QCD} ($\simeq 200$ MeV) is the QCD scale parameter, which can be determined, for example, by fitting Eq. (1.1) to the experimental data.

Another important feature of QCD is the dynamical generation of quark masses due to the condensation of quark–anti-quark pairs, the chiral condensates. Although the QCD Lagrangian has an approximated chiral symmetry in the light quark sector, this symmetry is spontaneously broken in the vacuum, or ground state, due to a non-vanishing chiral condensate. Therefore, the chiral condensate works as an order parameter for spontaneous chiral symmetry breaking.

Due to the difficulties to treat QCD with perturbation theory at energies relevant to nuclear physics, the development of alternative approximations is of utmost im-

portance. The most powerful non-perturbative method is the Monte-Carlo numerical simulation on the lattice, known as lattice QCD (LQCD). However, so far, its practical use at low temperatures and high chemical potentials is limited due to the *sign problem*. There are many non-perturbative models designed to mimic some aspects of QCD, but each one of them has its shortcomings. Nevertheless, using results found in each model, one is able to construct a presumable scenario for the QCD phase structure.

In this vein, the Nambu–Jona-Lasinio model (NJL) is one of the most successful effective theories used to describe interacting quarks. This model was proposed in 1961 in two papers by Yoichiro Nambu and Giovanni Jona-Lasinio who pursued analogies with superconductors [3, 4].

The standard version of the NJL model, which is non-renormalizable in $(3+1)$ dimensions, fails to describe the confinement of quarks because it does not consider gluons but this property can be enforced by adding the so called Polyakov loop to the standard NJL Lagrangian [5]. Then, with the Polyakov–Nambu–Jona-Lasinio model (PNJL) we can obtain thermodynamical quantities such as the pressure, the energy density, the entropy density, etc, in terms of two order parameters (one for chiral symmetry and the other for confinement) setting an appropriate framework to investigate the QCD phase transitions.

It is generally believed that effective theories used to describe compressed strongly interacting matter should include vector channels [2, 6–11] such as the ones which appear in the Walecka model for nuclear matter [12] and in the extended version of the NJL model for quark matter [13]. To emphasize its importance let us point out few recent applications which consider this channel in the framework of the NJL model starting with Ref. [14] where the three flavor version of this theory has been used to reproduce the equation of state (EoS) for cold magnetized quark matter [14]. In agreement with Ref. [15] the results show that the magnetic field and the vector channel tend to influence the first order chiral transition in opposite ways: while the first softens the EoS the second hardens it so that higher stellar masses may be reproduced giving further insight to the modeling of stellar objects such as the two recently measured pulsars, PSR J1614-2230 [16] and PSR J0348+0432 [17], whose masses are about $2M_{\odot}$. Another timely important application [18] shows that the presence of a vector interaction is crucial for the NJL to reproduce the measured relative elliptic flow differences between nucleons and anti-nucleons as well as between kaons and antikaons at energies carried out in the Beam-Energy Scan program of the Relativistic Heavy Ion Collider. As a final example, let us recall that although most investigations seem to support the QCD critical point (CP), an interesting observation against its existence has been advanced by de Forcrand and Philipsen [19] who, using numerical simulations of QCD at imaginary chemical potential, observed that the region of quark masses where the transition is presumably of the first order tends to shrink (for quark masses smaller than the physical ones) at small positive values of the chemical potential. On the other hand, evaluations which support the critical point existence indicate that this first order transition region should expand when the chemical potential increases so that the physical quark mass point hits the critical

line at some finite value of the temperature and chemical potential locating the CP position. A possible explanation for this disagreement has been given in Ref. [20] where it was suggested that a strong (repulsive) vector coupling may account for the initial shrinkage of the first order region, that would then start expanding again at larger values of the chemical potential, forcing the critical surface to bend back so that a CP naturally appears as the quark masses reach their physical values.

In practice, within the NJL model, a vector channel can be easily implemented by adding a term such as $-G_V(\bar{\psi}\gamma^\mu\psi)^2$ to the original lagrangian density. Then, within the mean field approximation (MFA), only the zeroth component survives so that the *net* effect produced by this channel is to add a term like $-G_V\rho^2$ to the pressure (ρ represents the quark number density) weakening (strengthening) the first order transition when G_V is positive (negative) [20]. As a result, in the repulsive case ($G_V > 0$), the first order transition region covers a smaller range of temperatures as compared to the $G_V = 0$ case while the coexistence chemical potential for a given temperature is shifted to a higher value. Then, as a consequence, the CP happens at smaller temperatures and higher chemical potentials than in the case of vanishing G_V.

1.1. The QCD phase diagram

Figure 1.1 summarizes the phase structure of QCD, which nowadays is constructed by schematic conjectures, constrained by a relatively small number of theoretical and empirical facts.

The QCD phase transition at finite temperatures and vanishing chemical potential has been studied extensively by LQCD. The results depend on the number of colors and flavors as expected from effective theories on the basis of the renormalization group as well as universality arguments [21, 22]. For three colors and the light flavors, LQCD analyses based on staggered fermions and Wilson fermions, indicated a crossover from the hadronic phase to the QGP for realistic u, d and s quark masses [23]. The pseudocritical temperature, T_{pc}, which characterizes the crossover location, is likely to be in the region $150 - 200$ MeV. At the same time, most of the chiral models suggest a critical point (second order phase transition) for the hadron-quark phase transition, where the chiral transition becomes first-order, for higher chemical potentials and a crossover for lower chemical potential values. Color superconductivity takes place at low temperatures and $\mu \gg \Lambda_{QCD}$, where QCD becomes analogous to condensed matter physics with “Cooper" pairs formed by quark-quark pairs.

1.2. The sign problem of QCD at finite densities

In order to evaluate the QCD partition function at finite chemical potentials one has to consider the determinant of the quark matrix, which is given by $\mathcal{M}(\mu) = \not{D} + m - \gamma_0\mu$. However, it turns out that this quantity, which is complex when μ is real and non-zero,

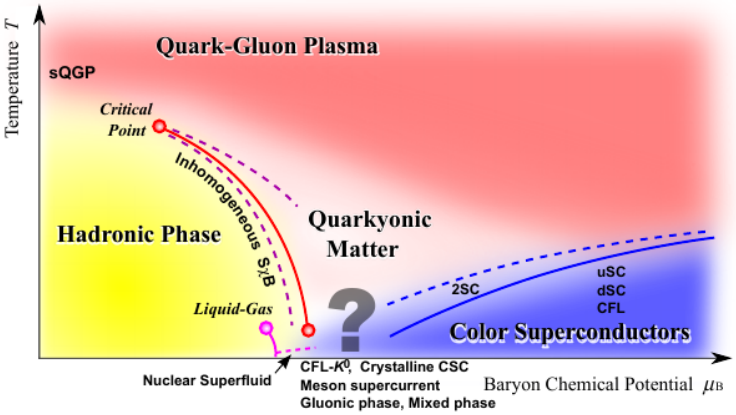

Figure 1.1.: Conjetured QCD phase diagram with transition boundaries between different states of matter. Figure taken from Ref. [24]

satisfies [25–28]

$$\det\left(\not{D} + m + \gamma_0\mu\right) = \det{}^*\left(\not{D} + m + \gamma_0\mu^*\right). \tag{1.2}$$

The above relation is complex if the real part of μ is finite. But since a complex determinant cannot be interpreted as a probability measure, the Monte Carlo method used by LQCD does not work, resulting in the QCD sign problem. Then, in order to study compressed quark matter, one has to consider an alternative such as the use of effective models which are simpler than pure QCD. Within LQCD, another possible approach is to consider μ to be an imaginary number and then to perform an analytic continuation back to the real μ-axis. Meanwhile, other LQCD workers prefer to apply a Taylor expansion in powers of μ/T around $\mu = 0$.

1.3. Scope and outline of this dissertation

The aim of the present work is to analyze the two-flavor PNJL model beyond the standard Large-N_c (LN) limit. This investigation is carried with the Optimized Perturbation Theory (OPT) and the results are compared with those furnished by the Large-N_c approximation and LQCD. We also show that the OPT radiatively generates a vector repulsive term as a finite N_c correction such as the one which appears in extended version of the NJL model for quark matter.

In chapter 2 we review the standard two-flavor NJL model, considering the OPT and the LN approximation. We use Feynman's formalism to obtain the effective potential and, with it, we analyze the thermodynamics of the system paying special attention to spontaneous chiral symmetry breaking in the vacuum, and its restoration

at finite T. Several thermodynamical quantities at zero chemical potential are studied and the vector repulsive term is introduced in the NJL model at the large-N_c limit.

In chapter 3 the Polyakov loop is introduced in order to simulate confinement and the results obtained with the PNJL model are compared with those furnished by the NJL model. Next, the second cumulant is calculated with the PNJL model using the OPT and the LN approximation (with $G_V = 0$ and with $G_V \neq 0$) and the results are compared with those furnished by LQCD.

In chapter 4 the entanglement vertex is added to the PNJL model via the Polyakov loop in order to decrease the scalar coupling constant, giving place to the so called entangled Polyakov–Nambu–Jona-Lasinio (EPNJL). The results obtained with this model using the OPT and the LN approximation are compared with LQCD data.

Finally, in chapter 5 the conclusions and future perspectives are presented.

2. The Nambu–Jona-Lasinio Model

In this chapter we will discuss the standard two flavor NJL model for quark matter using two different non perturbative methods: the large-N_c approximation and the Optimized Perturbation Theory.

2.1. The model and its symmetries

The two flavor NJL Lagrangian density can be written as [3]

$$\mathcal{L}_{NJL} = \bar{\psi}\left(i\partial\!\!\!/ - \hat{m}_0\right)\psi + G_S\left[\left(\bar{\psi}\psi\right)^2 + \left(\bar{\psi}i\gamma_5\boldsymbol{\tau}\psi\right)^2\right], \tag{2.1}$$

where ψ (sum over flavor and colour degrees of freedom is implicit) represents a isodoublet in flavor (u, d) and a N_c-plet quark field (N_c is the number of colors), $\boldsymbol{\tau}$ are the Pauli matrices and G_S represents the coupling strength. The quark mass matrix is $\hat{m}_0 = \mathrm{diag}\,(m_u, m_d)$, and we work in the isospin-symmetric limit $m_u = m_d = m_0$.

2.1.1. Chiral Symmetry

We say that an object is a chiral object when its image in a mirror cannot be superposed with the object. For example, when we see the image of our right hand in a mirror, it looks like our left hand and, since these two images cannot be superposed, we say that our hands are chiral objects. On the other hand, if we see the image of a sphere in a mirror, the image on the mirror can be superposed and we say that this object is a non-chiral object.

In physics fermions have an attribute called helicity that describes the projection of the spin in the direction of motion. When the projection of the spin is in the same direction of the motion, the fermion helicity is defined as being positive and, when the projection is in the opposite direction, the helicity is defined as being negative.

Suppose that a massive fermion particle has a positive helicity. Now, to an observer moving in the same direction but with a higher velocity, the same particle appears as having a negative helicity, which means that the helicity can be frame dependent. However, if the fermion is massless it moves at the speed of light so that helicity becomes a well defined quantity yielding the same eigenvalue in any reference frame.

The mathematical description of chirality can be done in terms of right (R) and left (L) projectors , P_R and P_L, defined as follows[29–33]

$$P_R = \left(\frac{1+\gamma^5}{2}\right), \quad P_L = \left(\frac{1-\gamma^5}{2}\right). \tag{2.2}$$

Right-handed means the projection of the spin and the momentum are in the same direction, and left-handed means projection of the spin in opposite direction to the momentum.

Now the quark field ψ can be decomposed into two chiral components,

$$\psi_R = P_R\psi, \quad \text{and} \quad \psi_L = P_L\psi, \tag{2.3}$$

and we can perform the chiral transformations

$$\psi_R \to \psi'_R = e^{i\frac{\boldsymbol{\tau}}{2}\cdot\boldsymbol{\theta}_R}\psi_R,$$

and

$$\psi_L \to \psi'_L = e^{i\frac{\boldsymbol{\tau}}{2}\cdot\boldsymbol{\theta}_L}\psi_L.$$

Then,

$$\psi \to \psi' = e^{i\frac{\boldsymbol{\tau}}{2}\cdot\boldsymbol{\theta}_R P_R} e^{i\frac{\boldsymbol{\tau}}{2}\cdot\boldsymbol{\theta}_L P_L}\psi, \tag{2.4}$$

where $\exp(i\boldsymbol{\tau}\cdot\boldsymbol{\theta}/2) \approx (1 + \boldsymbol{\tau}\cdot\boldsymbol{\theta}/2)$ and $\boldsymbol{\theta}$ is a free parameter. This is the transformation of the symmetry group $SU(2)_R \times SU(2)_L$.

It is more enlightening to change this transformation to a vector transformation and an axial transformation as follows

$$\begin{aligned} e^{i\frac{\boldsymbol{\tau}}{2}\cdot\boldsymbol{\theta}_R P_R} e^{i\frac{\boldsymbol{\tau}}{2}\cdot\boldsymbol{\theta}_L P_L}\psi &\to \left(1 + i\frac{\boldsymbol{\tau}}{2}\cdot\boldsymbol{\theta}_R P_R\right)\left(1 + i\frac{\boldsymbol{\tau}}{2}\cdot\boldsymbol{\theta}_L P_L\right)\psi \\ &= \left(1 + i\frac{\boldsymbol{\tau}}{2}\cdot\boldsymbol{\theta}_R P_R + i\frac{\boldsymbol{\tau}}{2}\cdot\boldsymbol{\theta}_L P_L\right)\psi + \mathcal{O}\left(\boldsymbol{\theta}^2\right) \\ &= \left[1 + i\frac{\boldsymbol{\tau}}{2}\cdot\left(\frac{\boldsymbol{\theta}_R + \boldsymbol{\theta}_L}{2}\right) + i\gamma^5\frac{\boldsymbol{\tau}}{2}\cdot\left(\frac{\boldsymbol{\theta}_R - \boldsymbol{\theta}_L}{2}\right)\right]\psi + \mathcal{O}\left(\boldsymbol{\theta}^2\right) \\ &= e^{i\frac{\boldsymbol{\tau}}{2}\cdot\boldsymbol{\theta}_V} e^{i\gamma^5\frac{\boldsymbol{\tau}}{2}\cdot\boldsymbol{\theta}_A}\psi, \end{aligned} \tag{2.5}$$

which is known as the $SU(2)_V \times SU(2)_A$ symmetry group. Now, we have a vector transformation

$$\Lambda_V: \quad \psi \to \psi' = e^{i\frac{\boldsymbol{\tau}}{2}\cdot\boldsymbol{\theta}_V}\psi \approx \left(1 + i\frac{\boldsymbol{\tau}}{2}\cdot\boldsymbol{\theta}_V\right)\psi, \tag{2.6}$$

$$\begin{aligned} \Lambda_V: \quad \bar{\psi} \to \left(\psi'\right)^\dagger\gamma^0 &= \left(\psi'\right)^\dagger e^{-i\frac{\boldsymbol{\tau}}{2}\cdot\boldsymbol{\theta}_V}\gamma^0 \\ &= \bar{\psi}e^{-i\frac{\boldsymbol{\tau}}{2}\cdot\boldsymbol{\theta}_V} \approx \bar{\psi}\left(1 - i\frac{\boldsymbol{\tau}}{2}\cdot\boldsymbol{\theta}_V\right), \end{aligned} \tag{2.7}$$

and an axial transformation

$$\Lambda_A: \quad \psi \to \psi' = e^{i\gamma^5\frac{\boldsymbol{\tau}}{2}\cdot\boldsymbol{\theta}_A}\psi \approx \left(1 + i\gamma^5\frac{\boldsymbol{\tau}}{2}\cdot\boldsymbol{\theta}_A\right)\psi, \tag{2.8}$$

$$\begin{aligned} \Lambda_A: \quad \bar{\psi} \to \left(\psi'\right)^\dagger\gamma^0 &= \left(\psi'\right)^\dagger e^{-i\gamma^5\frac{\boldsymbol{\tau}}{2}\cdot\boldsymbol{\theta}_A}\gamma^0 \\ &= \bar{\psi}e^{i\gamma^5\frac{\boldsymbol{\tau}}{2}\cdot\boldsymbol{\theta}_A} \approx \bar{\psi}\left(1 + i\gamma^5\frac{\boldsymbol{\tau}}{2}\cdot\boldsymbol{\theta}_A\right). \end{aligned} \tag{2.9}$$

It is easy to check that the Lagrangian density, Eq. (2.1), is invariant under the vector transformation. With this purpose, let us apply the axial transformation to each term appearing in the Lagrangian density. Then,

$$\begin{aligned}
\bar{\psi} i\gamma^\mu \partial_\mu \psi \to \left(\psi'\right)^\dagger \gamma^0 i\gamma^\mu \partial_\mu \psi' &= \bar{\psi} e^{i\gamma^5 \frac{\boldsymbol{\tau}}{2}\cdot\boldsymbol{\theta}_A} i\gamma^\mu \partial_\mu e^{i\gamma^5 \frac{\boldsymbol{\tau}}{2}\cdot\boldsymbol{\theta}_A}\psi \\
&= \bar{\psi}\left(1 + i\gamma^5 \frac{\boldsymbol{\tau}}{2}\cdot\boldsymbol{\theta}_A\right) i\gamma^\mu \left(1 + i\gamma^5 \frac{\boldsymbol{\tau}}{2}\cdot\boldsymbol{\theta}_A\right)\partial_\mu\psi \\
&= \bar{\psi} i\gamma^\mu \partial_\mu \psi - \bar{\psi}\gamma^5\gamma^\mu \frac{\boldsymbol{\tau}}{2}\cdot\boldsymbol{\theta}_A \partial_\mu\psi - \bar{\psi}\gamma^\mu\gamma^5 \frac{\boldsymbol{\tau}}{2}\cdot\boldsymbol{\theta}_A\partial_\mu\psi \\
&\quad + \mathcal{O}\left(\boldsymbol{\theta}_A^2\right) \\
&= \bar{\psi} i\gamma^\mu \partial_\mu \psi - \bar{\psi}\gamma^5\gamma^\mu \frac{\boldsymbol{\tau}}{2}\cdot\boldsymbol{\theta}_A \partial_\mu\psi + \bar{\psi}\gamma^5\gamma^\mu \frac{\boldsymbol{\tau}}{2}\cdot\boldsymbol{\theta}_A\partial_\mu\psi \\
&\quad + \mathcal{O}\left(\boldsymbol{\theta}_A^2\right) \\
&= \bar{\psi} i\gamma^\mu \partial_\mu \psi,
\end{aligned} \tag{2.10}$$

$$\begin{aligned}
\left(\bar{\psi}\psi\right)^2 \to \left(\left(\psi'\right)^\dagger \gamma^0 \psi'\right)^2 &= \left(\bar{\psi} e^{i\gamma^5 \frac{\boldsymbol{\tau}}{2}\cdot\boldsymbol{\theta}_A} e^{i\gamma^5 \frac{\boldsymbol{\tau}}{2}\cdot\boldsymbol{\theta}_A}\psi\right)^2 \\
&= \left(\bar{\psi}\psi + 2\bar{\psi} i\gamma^5 \frac{\boldsymbol{\tau}}{2}\cdot\boldsymbol{\theta}_A\psi\right)^2 \\
&= \left(\bar{\psi}\psi\right)^2 + 2\bar{\psi}\psi\bar{\psi} i\gamma^5 \frac{\boldsymbol{\tau}}{2}\cdot\boldsymbol{\theta}_A\psi + 2\bar{\psi} i\gamma^5 \frac{\boldsymbol{\tau}}{2}\cdot\boldsymbol{\theta}_A\psi\bar{\psi}\psi + \mathcal{O}\left(\boldsymbol{\theta}_A^2\right) \\
&= \left(\bar{\psi}\psi\right)^2 + 2\bar{\psi}\psi\bar{\psi} i\gamma^5 \frac{\boldsymbol{\tau}}{2}\cdot\boldsymbol{\theta}_A\psi - 2\bar{\psi}\psi\bar{\psi} i\gamma^5 \frac{\boldsymbol{\tau}}{2}\cdot\boldsymbol{\theta}_A\psi + \mathcal{O}\left(\boldsymbol{\theta}_A^2\right) \\
&= \left(\bar{\psi}\psi\right)^2,
\end{aligned} \tag{2.11}$$

$$\begin{aligned}
\left(\bar{\psi} i\gamma_5 \boldsymbol{\tau}\psi\right)^2 \to \left(\left(\psi'\right)^\dagger \gamma^0 i\gamma_5\boldsymbol{\tau}\psi'\right)^2 &= \left(\bar{\psi} e^{i\gamma^5 \frac{\boldsymbol{\tau}}{2}\cdot\boldsymbol{\theta}_A} i\gamma_5\boldsymbol{\tau} e^{i\gamma^5 \frac{\boldsymbol{\tau}}{2}\cdot\boldsymbol{\theta}_A}\psi\right)^2 \\
&= \left(\bar{\psi}\left(1 + i\gamma^5 \frac{\boldsymbol{\tau}}{2}\cdot\boldsymbol{\theta}_A\right) i\gamma_5\boldsymbol{\tau}\left(1 + i\gamma^5 \frac{\boldsymbol{\tau}}{2}\cdot\boldsymbol{\theta}_A\right)\psi\right)^2 \\
&= \left(\bar{\psi} i\gamma_5\boldsymbol{\tau}\psi - 2\bar{\psi}\frac{\boldsymbol{\tau}}{2}\cdot\boldsymbol{\theta}_A\boldsymbol{\tau}\psi + \mathcal{O}\left(\boldsymbol{\theta}^2\right)\right)^2 \\
&= \left(\bar{\psi} i\gamma_5\boldsymbol{\tau}\psi\right)^2 - 2\bar{\psi} i\gamma_5\boldsymbol{\tau}\psi\bar{\psi}\frac{\boldsymbol{\tau}}{2}\cdot\boldsymbol{\theta}_A\boldsymbol{\tau}\psi \\
&\quad - 2\bar{\psi}\frac{\boldsymbol{\tau}}{2}\cdot\boldsymbol{\theta}_A\boldsymbol{\tau}\psi\bar{\psi} i\gamma_5\boldsymbol{\tau}\psi + \mathcal{O}\left(\boldsymbol{\theta}^2\right) \\
&= \left(\bar{\psi} i\gamma_5\boldsymbol{\tau}\psi\right)^2 - 2\bar{\psi} i\gamma_5\boldsymbol{\tau}\psi\bar{\psi}\frac{\boldsymbol{\tau}}{2}\cdot\boldsymbol{\theta}_A\boldsymbol{\tau}\psi \\
&\quad + 2\bar{\psi} i\gamma_5\boldsymbol{\tau}\psi\bar{\psi}\frac{\boldsymbol{\tau}}{2}\cdot\boldsymbol{\theta}_A\boldsymbol{\tau}\psi + \mathcal{O}\left(\boldsymbol{\theta}^2\right) \\
&= \left(\bar{\psi} i\gamma_5\boldsymbol{\tau}\psi\right)^2.
\end{aligned} \tag{2.12}$$

Note that we have used the fact that $\boldsymbol{\tau}$ and γ^μ act on different spaces, so that they commute.

So far, all the terms in the Lagrangian density are invariant under $SU(2)_A$. Finally, let us see what happens with the mass term. A straightforward evaluation yields

$$\begin{aligned} m\bar{\psi}\psi \to m\left(\psi'\right)^{\dagger}\gamma^0\psi' &= m\bar{\psi}e^{i\gamma^5\frac{\boldsymbol{\tau}}{2}\cdot\boldsymbol{\theta}_A}e^{i\gamma^5\frac{\boldsymbol{\tau}}{2}\cdot\boldsymbol{\theta}_A}\psi \\ &= m\bar{\psi}\left(1+2i\gamma_5\boldsymbol{\tau}\psi\bar{\psi}\frac{\boldsymbol{\tau}}{2}\right)\psi \\ &= m\bar{\psi}\psi + 2mi\bar{\psi}\gamma_5\boldsymbol{\tau}\psi\bar{\psi}\frac{\boldsymbol{\tau}}{2}\psi, \end{aligned} \tag{2.13}$$

showing that, as expected, the presence of a massive term in the Lagrangian density breaks the chiral $SU(2)_A$ symmetry. In this case, we say that chiral symmetry is explicitly broken because the Lagrangian density is not chirally invariant.

Neutrons and protons have a mass of approximately 1 GeV so that the effective mass of up and down quarks within these baryons should be about 330 MeV. However, the bare (or current) mass of a light quark is about 5 MeV, thus the interaction between quarks gives mass to the neutrons and protons and, in general, to all hadrons. Then, even if one considers the current mass to be zero (exact chiral symmetry) the effective mass breaks the symmetry as the hadronic spectra shows. This is known as the chiral dynamical symmetry breaking mechanism.

2.2. The effective potential

In order to investigate how symmetry breaking occurs in a particular theory, one can analyze its free energy. For example, in statistical mechanics the free energy functional for a ferromagnetic material can be expressed as

$$F\left[\boldsymbol{M}\left(x\right)\right] = \int d^3x\left[\mathcal{E}\left(\boldsymbol{M}\left(x\right)\right) + \frac{1}{2}\boldsymbol{K}_T\left(\boldsymbol{M}\left(x\right)\right)\left(\boldsymbol{\nabla}\cdot\boldsymbol{M}\left(x\right)\right)^2 + \cdots\right], \tag{2.14}$$

where $\mathcal{E}$ is the free bulk energy density and K_T represents a constant while the magnetization, $\boldsymbol{M}(x)$, characterizes the order parameter for the phase transitions. The free energy described by Eq. (2.14) takes eventual inhomogeneities into account since $\boldsymbol{M}$ is position dependent but when the order parameter is constant the phase transitions can be described in terms of $\mathcal{E}(M)$ only. In quantum field theory (QFT), the phenomenon of symmetry breaking can be studied in terms of an analogous object, namely, the effective action [34]

$$\Gamma\left[\sigma\left(x\right)\right] = \int d^4x\left[-\mathcal{F}\left(\sigma\left(x\right)\right) + \frac{1}{2}Z_\sigma\left(\partial_\mu\sigma\right)^2 + \cdots\right], \tag{2.15}$$

where $\sigma\left(x\right)$ represents a (classical) scalar field, Z_σ represents a (renormalization) constant while $\mathcal{F}$ is known as the effective potential. In our case, we consider the order parameter to be independent of position and time ($\sigma\left(x\right) = \sigma$), which means that the system is composed by homogeneous and static infinite matter. In this case, the effective action is reduced to

$$\Gamma\left(\sigma\right) = -\int d^4x\mathcal{F}\left(\sigma\right), \tag{2.16}$$

and, the scalar field σ represents the order parameter for symmetry breaking.

To calculate the effective potential (or the Landau's free energy), one can use the path integral formalism. Within this approach the partition function, $\mathcal{Z}$, can be written in terms of the effective potential as follows (for details see Refs. [34, 35]):

$$\mathcal{Z} = \exp\left[-i\int d^4x\mathcal{F}\right]. \tag{2.17}$$

Then, as within statistical mechanics, all the relevant thermodynamical quantities, such as the pressure, can easily be obtained once the free energy (or the partition function) is known. However, the complete evaluation of $\mathcal{F}$ is an impossible task within most interacting theories so that one needs to invoke an approximation scheme, such as the OPT or the LN approximation studied here.

Before solving Eq. (2.17), for the NJL model case it is convenient to write down the Lagrangian density in terms of the auxiliary fields, σ and $\boldsymbol{\pi}$, by using the Hubbard-Stratanovich transformation, which consists in adding the following quadratic terms to the Lagrangian density:

$$\Theta^2 = -\frac{1}{G_S}\left[\frac{\sigma}{2} + G_S\left(\bar{\psi}\psi\right)\right]^2, \quad \Omega^2 = -\frac{1}{G_S}\left[\frac{\boldsymbol{\pi}}{2} + G_S\left(\bar{\psi}i\gamma_5\boldsymbol{\tau}\psi\right)\right]^2. \tag{2.18}$$

Then, the the original theory can be written in a bosonized fashion as

$$\mathcal{L}_{NJL} = \bar{\psi}\left(i\partial\!\!\!/ - m_0\right)\psi - \frac{1}{4G_S}\left(\sigma^2 + \boldsymbol{\pi}^2\right) - \bar{\psi}\left[\sigma + i\gamma_5\boldsymbol{\pi}\cdot\boldsymbol{\tau}\right]\psi. \tag{2.19}$$

Applying the Euler-Lagrange equations to the Lagrangian density for the auxiliary fields σ and $\boldsymbol{\pi}$, we get

$$\sigma = -2G_S\bar{\psi}\psi \quad \text{and} \quad \boldsymbol{\pi} = -2G_S\bar{\psi}i\gamma_5\boldsymbol{\tau}\psi, \tag{2.20}$$

which means that Θ^2 and Ω^2 are equal to zero. Note that within the bosonized theory the interactions are described by Yukawa vertices while the σ and $\boldsymbol{\pi}$ fields do not propagate. This version is advantageous if one wants to apply the large N_c approximation since, in this case, $G_S \to G_S/N_c$ which means that the mesonic propagators carry a $1/N_c$ factor while a closed fermionic loop contributes with a factor N_c. Then, the counting of $1/N_c$ powers can be easily carried out [36].

2.2.1. The interpolated model

To implement the OPT approximation (also known as *linear delta expansion*, LDE, see [37, 38] for earlier references) in the NJL model we follow Ref. [39].

Basically, this method consists in modifying the Lagrangian of a particular theory by introducing a dummy expansion parameter, δ.

Let $\mathcal{L}$ be the original Lagrangian density we want to solve, and $\mathcal{L}_0$ a Lagrangian density of a free theory that we know how to solve exactly. Then, the Lagrangian density in terms of δ can be written as

$$\mathcal{L}(\delta) = (1-\delta)\mathcal{L}_0 + \delta\mathcal{L} = \mathcal{L}_0 + \delta\left(\mathcal{L} - \mathcal{L}_0\right). \tag{2.21}$$

As one can easily see, $\mathcal{L}(\delta)$ interpolates between the original theory ($\delta = 1$) and a free (exactly solvable) theory ($\delta = 0$). Then, the relevant physical quantities are evaluated as a power series in δ, which is formally treated as a small number.

It is is crucial to note that for dimensional balance, the Lagrangian density $\mathcal{L}_0$ must have at least one arbitrary mass parameter (η). This is a welcome fact since η will act as an infra red regulator if the original theory is massless. One can then fix the arbitrary η by requiring that any physical quantity $\mathcal{P}(\eta)$, be at least locally η-independent. This optimization criterion translates into the following variational condition

$$\left.\frac{\partial \mathcal{P}(\eta)}{\partial \eta}\right|_{\bar{\eta}} = 0, \tag{2.22}$$

which is known as the *principle of minimal sensitivity* (PMS) [40]. The solution of the PMS equation gives $\bar{\eta}$ as a function of the original parameters of the theory. The convergence of the OPT in the case of critical theories is given in Ref. [41].

The OPT has already established itself as a powerful method in dealing with critical theories. For example, in the Bose-Einstein condensation case this method and its different variations have provided some of the most precise analytical results for the shift in the critical temperature for weakly interacting homogeneous Bose gases [42, 43]. Other applications to condensed matter situations include a precise evaluation of the critical density for polyacetylene [44]. Also, when extended by hard-thermal loops, the method was successful in predicting QCD thermodynamical properties at the three-loop level [45]. Improved by the renormalization group (RG), and inspired by similar properties [46] in the Gross-Neveu model, a variation of the OPT has been recently used in the evaluation of $\Lambda_{\overline{\text{MS}}}^{\text{QCD}}$ [47] and α_S [48], where the stability and convergence at higher orders of this RG-OPT form was demonstrated.

Now, in order to apply this method to the NJL Lagrangian density, Eq. (2.19), one can define the quadratic term, $\mathcal{L}_0$, as

$$\mathcal{L}_0 = \bar{\psi}\left(i\partial\!\!\!/ - m_0 - \eta\right)\psi.$$

Then, following the OPT interpolation prescription, Eq. (2.21), one gets

$$\begin{aligned}\mathcal{L}_{NJL}(\delta) =& \bar{\psi}\left(i\partial\!\!\!/ - m_0 - \eta\right)\psi \\ &+ \delta\left[\eta\bar{\psi}\psi - \frac{1}{4G_S}\left(\sigma^2 + \boldsymbol{\pi}^2\right) - \left(\sigma\bar{\psi}\psi + \bar{\psi}i\gamma_5\boldsymbol{\pi}\cdot\boldsymbol{\tau}\psi\right)\right].\end{aligned} \tag{2.23}$$

To compare the OPT results with the ones furnished by the LN approximation it is convenient to take $G_S \to \lambda/(2N_c)$ so that to each Yukawa vertex contributes with a $1/N_c$ factor. Note that, within the LN approximation, the number of colors, N_c, is formally treated as a large number which is set to 3 at the end.

It is easy to see that Eq. (2.23) can be written as

$$\mathcal{L}_{NJL}(\delta) = \bar{\psi}\left[i\partial\!\!\!/ - m_0 - \delta\left(\sigma + i\gamma_5\boldsymbol{\pi}\cdot\tau\right) - \eta\left(1-\delta\right)\right]\psi - \delta\frac{N_c}{2\lambda}\left(\sigma^2 + \boldsymbol{\pi}^2\right). \tag{2.24}$$

To order δ, the effective potential is given by the Feynman diagrams shown in Fig. 2.1, where the mass term appearing in the OPT dressed propagators is defined by [49]

$$\hat{\eta} = \eta + m_0 - \delta\left[\eta - (\sigma + i\gamma_5 \boldsymbol{\pi}\cdot\boldsymbol{\tau})\right]. \tag{2.25}$$

so that all the η, σ and $\boldsymbol{\pi}$ insertions are automatically accounted for.

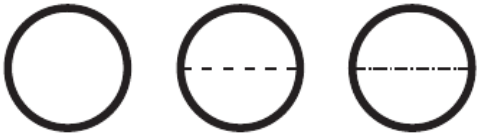

Figure 2.1.: Diagrams contributing to $\mathcal{F}(\hat{\eta})$ to order δ. The thick continuous lines represent the OPT dressed fermionic propagators, the dashed line represents the σ propagator and the dashed-doted line represents the π propagator (Figure taken from Ref. [49])

Applying the Feynman rules one then obtains [49]

$$\begin{aligned}\mathcal{F} =& \frac{N_c}{2\lambda}\left(\sigma^2 + \boldsymbol{\pi}^2\right) + i\int\frac{d^4p}{(2\pi)^4}\mathrm{Tr}\ln\left(\not{p} - \hat{\eta}\right)\\ &+ \delta\frac{\lambda}{2N_c}\int\frac{d^4p}{(2\pi)^4}\int\frac{d^4q}{(2\pi)^4}\mathrm{Tr}\left[\left(\frac{\not{p}+\hat{\eta}}{p^2-\hat{\eta}^2}\right)\left(\gamma_5\tau_i\frac{\not{q}+\hat{\eta}}{q^2-\hat{\eta}^2}\gamma_5\tau_i\right)\right]\\ &- \delta\frac{\lambda}{2N_c}\int\frac{d^4p}{(2\pi)^4}\int\frac{d^4q}{(2\pi)^4}\mathrm{Tr}\left[\left(\frac{\not{p}+\hat{\eta}}{p^2-\hat{\eta}^2}\right)\left(\frac{\not{q}+\hat{\eta}}{q^2-\hat{\eta}^2}\right)\right].\end{aligned} \tag{2.26}$$

It is clear that (after taking the trace over colors) the first two terms are of order N_c while the last two, which are of order N_c^0, would not contribute to a LN type of calculation. This important remark emphasizes the fact that already at the first non-trivial order the OPT considers terms which belong to the NLO (next to the leading order) order in a $1/N_c$ type of expansion. Here, the first $1/N_c$ corrections due to the OPT type of expansion have the topology of exchange (Fock) type of diagrams as Fig. 2.1 explicitly shows.

The mass term $\hat{\eta}$ is dressed by the scalar field σ and the pseudoescalar field $\boldsymbol{\pi}$ and, in order to maintain the Goldstone structure of the theory [38, 50], it must be defined as [38]

$$\eta = \alpha + i\gamma_5\boldsymbol{\nu}\cdot\boldsymbol{\tau}, \tag{2.27}$$

where $\boldsymbol{\nu}$ is a three-vector.

Now the PMS conditions to be satisfield at $\delta = 1$ are

$$\left.\frac{\partial \mathcal{F}}{\partial \alpha}\right|_{\bar{\alpha},\bar{\nu}_i} = 0 \quad \text{and} \quad \left.\frac{\partial \mathcal{F}}{\partial \nu_i}\right|_{\bar{\alpha},\bar{\nu}_i} = 0. \tag{2.28}$$

Identifying

$$\begin{aligned} A &= \gamma^\mu p_\mu - \hat{\eta} \\ &= \begin{pmatrix} p_0 - a & 0 & -p_3 - b & -p_1 + ip_2 \\ 0 & p_0 - a & -p_1 - ip_2 & p_3 - b \\ p_3 - b & p_1 - ip_2 & -p_0 - a & 0 \\ p_1 + ip_2 & -p_3 - b & 0 & -p_0 - a \end{pmatrix} \end{aligned} \tag{2.29}$$

and

$$\begin{aligned} B &= \gamma^\mu p_\mu + \hat{\eta} \\ &= \begin{pmatrix} p_0 + a & 0 & -p_3 - b & -p_1 + ip_2 \\ 0 & p_0 + a & -p_1 - ip_2 & p_3 - b \\ p_3 - b & p_1 - ip_2 & -p_0 + a & 0 \\ p_1 + ip_2 & -p_3 - b & 0 & -p_0 + a \end{pmatrix}, \end{aligned} \tag{2.30}$$

where $a = \alpha(1-\delta) - m - \delta\sigma$ and $b = i\boldsymbol{\nu}\cdot\boldsymbol{\tau}(1-\delta) - i\delta\boldsymbol{\pi}\cdot\boldsymbol{\tau}$. One can use the identity $\mathrm{Tr}\ln = \ln\det$, to expand the logarithm to order δ. Then, by taking the trace in each one of the integrals in Eq. (2.26) one gets

$$\begin{aligned} \frac{\mathcal{F}}{N_c} =& \frac{1}{2\lambda}\left(\sigma^2 + \boldsymbol{\pi}^2\right) + 2iN_f \int \frac{d^4p}{(2\pi)^4} \ln\left[-p^2 + (\alpha + m_0)^2 + \boldsymbol{\nu}^2\right] \\ &+ 4i\delta N_f \int \frac{d^4p}{(2\pi)^4} \frac{(\alpha + m_0)(\alpha - \sigma) + \boldsymbol{\nu}(\boldsymbol{\nu} - \boldsymbol{\pi})}{-p^2 + \hat{\eta}^2} \\ &- 2(n_\pi + 1)\delta \frac{\lambda N_f}{N_c} \int \frac{d^4p}{(2\pi)^4} \frac{d^4q}{(2\pi)^4} \frac{p_\mu q^\mu}{(-p^2 + \hat{\eta})(-q^2 + \hat{\eta})} \\ &+ 2(n_\pi - 1)\delta \frac{\lambda N_f}{N_c} \int \frac{d^4p}{(2\pi)^4} \frac{d^4q}{(2\pi)^4} \frac{(\alpha + m_0)^2 - \boldsymbol{\nu}^2}{(-p^2 + \hat{\eta})(-q^2 + \hat{\eta})}, \end{aligned} \tag{2.31}$$

where n_π represents the number of pseudoescalars. In the $U(1)$ version of the model, where $N_f = 1$ and $n_\pi = 1$, so that the last term does not contribute and the OPT will bring $1/N_c$ corrections only at finite chemical potential, since the other correction term is related to the quark number density, which is zero at vanishing chemical potential. In our case, $n_\pi = 3$ and finite N_c corrections are expected to occur at any regime of density and/or temperature.

Applying the PMS equation for α and ν_i leads to a cumbersome problem, which can be circumvented by noticing the symmetry between α and ν_i, which allows us to select the σ direction and set $\pi_i = 0$, implying that $\bar{\nu}_i = 0$ [38] and $\bar{\alpha} = \bar{\eta}$. We also

note that in the third term of Eq. (2.31) only the zeroth component will eventually survive (when $\mu \neq 0$). Then, one finally gets

$$\begin{aligned}\frac{\mathcal{F}}{N_c} = \frac{\sigma^2}{2\lambda} &+ 2iN_f \int \frac{d^4p}{(2\pi)^4} \ln\left[-p^2 + (\eta - m_0)^2\right] \\ &+ 4i\delta N f \int \frac{d^4p}{(2\pi)^4} \frac{(\eta + m_0)(\eta - \sigma)}{-p^2 + (\eta + m_0)^2} \\ &- 8\delta \frac{\lambda N_f}{N_c} \left[\int \frac{d^4p}{(2\pi)^4} \frac{p_0}{-p^2 + (\eta + m_0)^2}\right]^2 \\ &+ 4\delta \frac{\lambda N_f}{N_c} (\eta + m_0)^2 \left[\int \frac{d^4p}{(2\pi)^4} \frac{1}{-p^2 + (\eta + m_0)^2}\right]^2 . \end{aligned} \tag{2.32}$$

Let us now use the Matsubara's (imaginary time) formalism in order to introduce the control parameters T and μ. Basically within this formalism, the time component is replaced by the temperature since the evolution of the system follows a path where each point of the path is a equilibrium state.

Since we are working with fermions, the solution of the Dirac equation must be anti-periodic in time $\psi(0, \boldsymbol{x}) = -\psi(\beta, \boldsymbol{x})$ [51], where $\beta = 1/T$.

Now one makes the substitution $p_0 \to i\omega_n + \mu$, where

$$\omega_n = \frac{(2n+1)\pi}{\beta}, \tag{2.33}$$

are the Matsubara frequencies for fermions, μ is the chemical potential (which is roughly related to the difference between particles and antiparticles) and $n = 0 \pm 1 \pm 2 ... \pm \infty$. Then replacing p_0 one obtains

$$\int \frac{d^4p}{(2\pi)^4} \to i \int d\omega_n \frac{d^3p}{(2\pi)^4}. \tag{2.34}$$

This is only valid when $T \to 0$, since $\Delta\omega_n = 2\pi T \Delta n \to 0$. Nevertheless, at finite T, the integral over ω_n in equation (2.34) becomes discretized as $T\Delta n$ becomes finite [52] and one can write

$$d\omega_n \to 2\pi T \sum_{n=-\infty}^{\infty},$$

so that

$$\int \frac{d^4p}{(2\pi)^4} \to \frac{i}{\beta} \int \frac{d^3p}{(2\pi)^3} \sum_{n=-\infty}^{\infty}. \tag{2.35}$$

In this case, Eq. (2.32), with $p = (i\omega_n + \mu, \boldsymbol{p})$, becomes

$$\begin{aligned}\frac{\mathcal{F}}{N_c} = &\frac{\sigma^2}{2\lambda} - \frac{2N_f}{\beta}\int\frac{d^3p}{(2\pi)^3}\sum_{n=-\infty}^{\infty}\ln\left[(\omega_n - i\mu)^2 + \boldsymbol{p}^2 + (\eta - m_0)^2\right] \\ &+ \delta\frac{4Nf}{\beta}\int\frac{d^3p}{(2\pi)^3}\sum_{n=-\infty}^{\infty}\frac{(\eta + m_0)(\eta - \sigma)}{(\omega_n - i\mu)^2 + \boldsymbol{p}^2 + (\eta + m_0)^2} \\ &+ 8\delta\frac{\lambda N_f}{\beta^2 N_c}\left[\int\frac{d^3p}{(2\pi)^3}\sum_{n=-\infty}^{\infty}\frac{\omega_n - i\mu}{(\omega_n - i\mu)^2 + \boldsymbol{p}^2 + (\eta + m_0)^2}\right]^2 \\ &- 4\delta\frac{\lambda N_f}{\beta^2 N_c}(\eta + m_0)^2\left[\int\frac{d^3p}{(2\pi)^3}\sum_{n=-\infty}^{\infty}\frac{1}{(\omega_n + i\mu)^2 + \boldsymbol{p}^2 + (\eta + m_0)^2}\right]^2, \end{aligned} \tag{2.36}$$

where the detailed evaluation of Matsubara's sums are given in appendix B.

Finally, we can write the effective potential in terms of temperature and chemical potential in the more compact form

$$\begin{aligned}\mathcal{F}(\eta, \sigma, \mu, T) = &\frac{\sigma^2}{4G_S} - 2N_f N_c I_1(\mu, T) + 2\delta N_f N_c(\eta + m_0)(\eta - \sigma) I_2(\mu, T) \\ &+ 4\delta G_S N_f N_c I_3^2(\mu, T) - 2\delta G_S N_f N_c(\eta + m_0)^2 I_2^2(\mu, T), \end{aligned} \tag{2.37}$$

where we have replaced $\lambda \to 2G_S N_c$. In the above equation we have also defined, for convenience, the integrals

$$I_1(\mu, T) = \int\frac{d^3p}{(2\pi)^3}\left\{E_p + \frac{1}{\beta}\ln\left[1 + e^{-\beta(E_p + \mu)}\right] + \frac{1}{\beta}\ln\left[1 + e^{-\beta(E_p - \mu)}\right]\right\}, \tag{2.38}$$

$$I_2(\mu, T) = \int\frac{d^3p}{(2\pi)^3}\frac{1}{E_p}\left[1 - f^+ - f^-\right] \tag{2.39}$$

and

$$I_3(\mu, T) = \int\frac{d^3p}{(2\pi)^3}\left[f^+ - f^-\right], \tag{2.40}$$

where $E_p^2 = \boldsymbol{p}^2 + (\eta + m_0)^2$ is the dispersion while

$$f^+ = \frac{1}{e^{\beta(E_p - \mu)} + 1}, \tag{2.41}$$

$$\tag{2.42}$$

and

$$f^- = \frac{1}{e^{\beta(E_p + \mu)} + 1}, \tag{2.43}$$

represent the fermion distribution functions for particles and antiparticles respectively.

The physical interpretation of the OPT free energy, Eq. (2.37), becomes clear by analyzing the physical meaning of each term. The first term represents the classical potential while the second is similar to the standard result obtained in the case of free fermionic gas whose masses are given by $m_0+\eta$ as I_1 suggests. The terms proportional to $I_2 \sim \partial I_1/\partial\eta$ are reminiscent of the one loop scalar density, $\rho_s = \langle\bar{\psi}\psi\rangle$. At the same time, the terms proportional to $I_3 \sim \partial I_1/\partial\mu$ only survive when $\mu \neq 0$ as Eq. (2.40) shows. This can be easily understood by recalling that, to one loop, the quark number density $\rho = \langle\psi^+\psi\rangle$ is given by I_3. Then, by noting that I_3 is $1/N_c$ suppressed one can readily draw the basic physical differences between the OPT and LN (or MF) approximations at this first non-trivial order. Namely, the OPT free energy is written in terms of scalar and vector condensates while only the scalar density contributes to the later. This observation is crucial for the discussions to be carried out in the sequel.

An important remark, at this point, is that the integrals for the vacuum state ($T = \mu = 0$) are divergent and, in typical NJL evaluations, they are usually regulated by a sharp non-covariant ultra violet momentum cut-off, Λ, which cannot be removed by a systematic redefinition of the *original* parameters as in a renormalizable theory. To deal with this situation one generally considers Λ to be a new "parameter" which sets the maximum energy scale at which the model predictions can be trusted. Then, the vacuum integrals in terms of the cut-off Λ read

$$\begin{aligned} I_1(0,0) &= \int \frac{d^3p}{(2\pi)^3} E_p \\ &= -\frac{1}{32\pi^2}\left\{(\eta+m_0)^4 \ln\left[\frac{\left(\Lambda+\sqrt{\Lambda^2+(\eta+m_0)^2}\right)^2}{(\eta+m_0)^2}\right]\right. \\ &\quad \left. -2\sqrt{\Lambda^2+(\eta+m_0)^2}\left[2\Lambda^3+\Lambda(\eta+m_0)^2\right]\right\}, \end{aligned} \tag{2.44}$$

and

$$\begin{aligned} I_2(0,0) &= \int \frac{d^3p}{(2\pi)^3}\frac{1}{E_p} \\ &= \frac{1}{4\pi^2}\left\{\Lambda\sqrt{\Lambda^2+(\eta+m_0)}-\frac{(\eta+m_0)^2}{2}\ln\left[\frac{\left(\Lambda+\sqrt{\Lambda^2+(\eta+m_0)^2}\right)^2}{(\eta+m_0)^2}\right]\right\}. \end{aligned} \tag{2.45}$$

Applying the PMS equation, (2.22), and noting that

$$\frac{\partial I_1}{\partial \eta} = (\eta + m_0)\, I_2 \tag{2.46}$$

we get for $\bar{\eta}$

$$\left\{ \left[\eta - \sigma - 2\,(\eta + m_0)\, G_S I_2\right] \left[1 + (\eta + m_0)\, \frac{\partial}{\partial \eta}\right] I_2 + 4 G_S I_3 \frac{\partial I_3}{\partial \eta} \right\}_{\eta = \bar{\eta}} = 0. \tag{2.47}$$

Since we are interested in the thermodynamic quantities such as the pressure, we must obtain the equilibrium condition for the effective potential

$$\left. \frac{\partial \mathcal{F}\,(\eta, \sigma, \mu, T)}{\partial \sigma} \right|_{\bar{\sigma}} = 0, \tag{2.48}$$

which gives the gap equation

$$\bar{\sigma} = 4 G N_f N_c\, (\eta + m_0)\, I_2. \tag{2.49}$$

In the LN limit the two terms proportional to G_S in Eq. (2.47) do not contribute and the PMS equation has as solutions $\bar{\eta} = \bar{\sigma}$ and $I_2 = (m_0 + \eta)\, \partial I_2 / \partial \eta$. However, the last solution only depends on Λ and η, and as a consequence does not have information about the theory itself. Therefore, in the large-N_c limit the solution $\bar{\eta} = \bar{\sigma}$ is usually considered as the physical one. With this, we reproduce the familiar expression for $\mathcal{F}$ in the LN approximation

$$\mathcal{F}_{LN}\,(\sigma, \mu, T) = \frac{\sigma^2}{4 G_S} - 2 N_f N_c I_1\,(\mu, T)\,, \tag{2.50}$$

showing how the OPT reproduces the "exact" result once the $N_c \to \infty$ limit is appropriately taken. This exercise helps to establish the reliability of the OPT method.

Having obtained the values of $\bar{\sigma}$ and $\bar{\eta}$ we can evaluate the pressure which is related to the free energy through

$$P = -\mathcal{F}\,(\bar{\eta}, \bar{\sigma}, \mu, T)\,. \tag{2.51}$$

Then, other important physical quantities such as the density energy ϵ and the interaction measure (or trace anomaly) Δ become available upon considering

$$\epsilon = -P + Ts + \mu\rho, \tag{2.52}$$

$$\Delta = \frac{\epsilon - 3P}{T^4}, \tag{2.53}$$

where s is the entropy density and ρ is the quark number density

$$s = \left(\frac{\partial P}{\partial T}\right)_{\mu}, \tag{2.54}$$

$$\rho = \left(\frac{\partial P}{\partial \mu}\right)_{T}. \tag{2.55}$$

Within the two flavor version of the NJL model there are three parameters to be fixed: the current mass m_0, the cut-off Λ and the coupling constant G_S.Usually they are adjusted so as to reproduce physical observables such as the pion mass ($m_\pi \simeq 135$ MeV), the pion decay constant ($f_\pi \simeq 92.4$ MeV) and the quark condensate ($-\langle\bar{\psi}\psi\rangle^{1/3} \simeq 250$ MeV) [33]. The (non-observable) current quark mass is related to the observables via the Gell–Mann-Oakes-Renner (GMOR) relation [53],

$$m_0 = \frac{-f_\pi^2 m_\pi^2}{2\langle\bar{\psi}\psi\rangle}. \tag{2.56}$$

There is a family of parameter sets tailored to reproduce the numerical values of these physical observables and, in general, one chooses a set which also reproduces the vacuum effective quark mass, $M = m_0 + \Sigma \simeq 330$ MeV, where Σ represents the self energy.

The parameter sets adopted in this work are given in table 2.1 (see Ref. [49] for other possibilities).

Table 2.1.: Parameter set for the OPT and for the LN approximation as given in Ref. [49]. These values were obtained to reproduce $m_\pi = 135$ MeV, $f_\pi = 92.4$ MeV and $-\langle\bar{\psi}\psi\rangle^{1/3} = 250$ MeV.

	Λ [MeV]	m_0 [MeV]	$G_S\Lambda^2$
OPT	640	4.9	1.99
LN	640	5.2	2.14

2.3. Results at finite temperature and zero density

As previously remarked, in the case of of vanishing density ($\mu = 0$) we have $I_3 = 0$, and the PMS condition, Eq. (2.47), becomes much simpler. Considering the PMS physical solution together with the gap equation, (2.49), one then obtains

$$\begin{aligned}\bar{\eta} &= \bar{\sigma} + 2G_S\left(\bar{\eta} + m_0\right) I_2 \\ &= \bar{\sigma}\left(1 + \frac{1}{2N_f N_c}\right),\end{aligned} \tag{2.57}$$

which corrects the LN relation $\bar{\eta} = \bar{\sigma}$.

Figure 2.2 displays the normalized effective potential for the physical case, $m_0 \neq 0$, and for the chiral limit, $m_0 = 0$. We see that in the chiral limit, the effective potential is symmetric, while in the physical case there is a small asymmetry which is due to the finite mass of the pion. In the chiral limit, where the symmetry is exact, the pion would represent the Goldstone boson of the theory but, in the real world, the

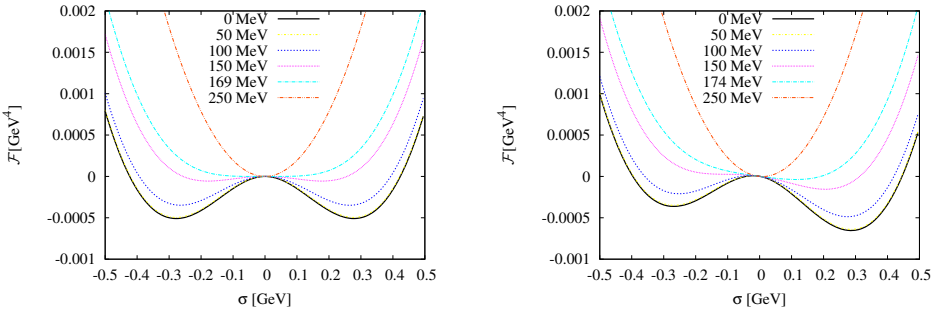

Figure 2.2.: OPT Effective potential as a function of σ at different temperatures for $\mu = 0$. *Left panel*: the chiral limit, $m_0 = 0$. *Right panel*: the physical case, $m_0 = 4.8$ MeV

pion represents a pseudo-Golstone boson whose mass is much smaller than the sigma meson mass ($m_\sigma \sim 600$ MeV) or the nucleon mass ($M_N \sim 1$ GeV).

The equilibrium state for small temperature signals a non-vanishing value for the order parameter, $\bar{\sigma}$, so that the quark effective mass is $M = m_0 + \bar{\sigma} \sim 330$ MeV as Fig. 2.2 shows. So, in the vacuum state, we have a finite effective mass even when $m_0 = 0$ when chiral symmetry is dynamically broken. As the temperature is increased, the equilibrium state is located at $\bar{\sigma} = 0$ ($\bar{\sigma} \simeq 0$), and chiral symmetry is (partially) restored in the chiral (physical) limit.

Next, using Eq. (2.57), one only needs to solve the gap equation (2.49) to obtain the order parameter, $\bar{\sigma}$, which controls the chiral transition. The critical (pseudocritical) temperature, T_c (T_{pc}), where the chiral transition occurs, in other words, where chiral symmetry is (partially) restored is found from the discontinuity (maximum) value of the thermal susceptibility, $-d\sigma/dT$.

Figure 2.3 shows the effective mass as a function of T/T_σ, where T_σ represents T_c or T_{pc}. The critical temperature is 169 MeV and 165 MeV in the chiral limit for the OPT and for the LN approximation respectively. In the physical case, the pseudocritical critical temperature is 174 MeV for the OPT and 172 MeV for the LN approximation.

In the chiral limit, we have a second order phase transition, while in the physical case we have a crossover [54, 55]. In a second order phase transition the thermal susceptibility (second derivative of the free energy) diverges in the critical point, while in a crossover we cannot strictly speak of a phase transition since the system goes continuously from one phase to another. This distinction becomes clear in Fig. 2.4 which displays the thermal susceptiblity as a function of T for each case and shows that this quantity clearly diverges only in the chiral limit. In this limit the effective mass becomes zero at the critical temperature and the chiral symmetry is restored, while in the physical case drops to the values close to m_0 at temperatures higher than

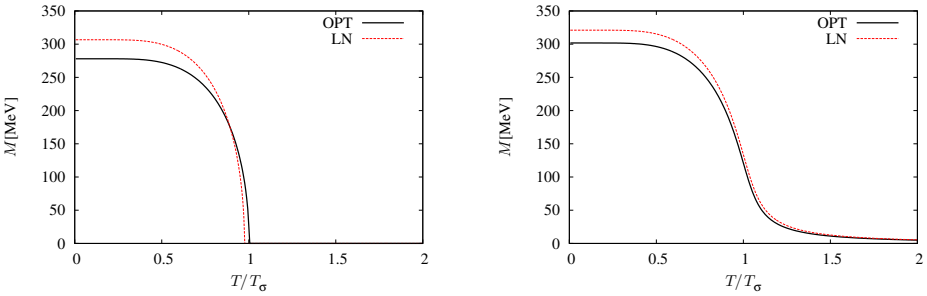

Figure 2.3.: The effective quark mass, M, as a function of T/T_σ for $\mu = 0$. *Left panel*: $m_0 = 0$. *Right panel*: $m_0 \neq 0$.

T_σ and we say that the system reaches an almost chirally symmetric phase.

Figure 2.5 shows the normalized pressure

$$P_N\left(\bar{\eta}, \bar{\sigma}, \mu, T\right) = P\left(\bar{\eta}, \bar{\sigma}, \mu, T\right) - P\left(\bar{\eta}, \bar{\sigma}, 0, 0\right), \tag{2.58}$$

in units of T^4. The above subtraction procedure, which is commonly adopted, means that $P_N = 0$ at $T = 0 = \mu$. For simplicity, we will drop the subscript N from now on.

Both, the OPT and the LN approximation predict the same behavior for P at $\mu = 0$, which shows the robustness of the LN approximation when only thermal effects are considered. This means that the OPT does not produce notorious changes in the pressure at zero chemical potential, which is not so surprising if one recalls that the term associated with $\langle \psi^+ \psi \rangle$ (I_3) does not contribute in this case.

Figure 2.6 shows the trace anomaly obtained with the OPT and with the LN approximation. The former predicts a slightly higher interaction at the crossover region.

2.3.1. Taylor expansion coefficients

The statistical moments, commonly determined from a measured multiplicity distribution, are the mean (M), the variance (σ^2) (not be confused with the scalar field), the skewness (S) and the kurtosis (κ). They are related to the (net-)number N of interest by $M = \langle N \rangle$, $\sigma^2 = \left\langle (\Delta N)^2 \right\rangle$, $S = \left\langle (\Delta N)^3 \right\rangle / \sigma^3$ and $\kappa = \left\langle (\Delta N)^4 \right\rangle / \sigma^4 - 3$ where $\Delta N = N - \langle N \rangle$ is the fluctuation of N around its mean value. The cumulants c_n of the distribution are defined as $c_1 = M$, $c_2 = \sigma^2$, $c_3 = S\sigma^3$, and $c_4 = \kappa\sigma^4$ and are, for an equilibrated system, related to generalized susceptibilities given by appropriate derivatives of the pressure. Studying fluctuations in statistical systems is important from several points of view. For instance, fluctuations define the stability of the system and its way of reaching the state of thermodynamic equilibrium [56]

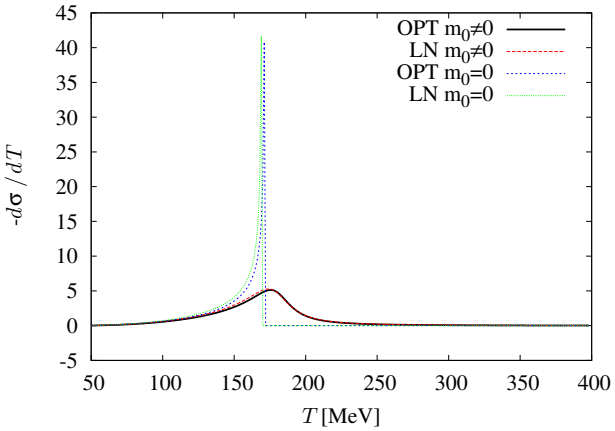

Figure 2.4.: Thermal susceptibility as a function of T at $\mu = 0$ in the chiral limit and in the physical case obtained with the OPT and the LN approximation

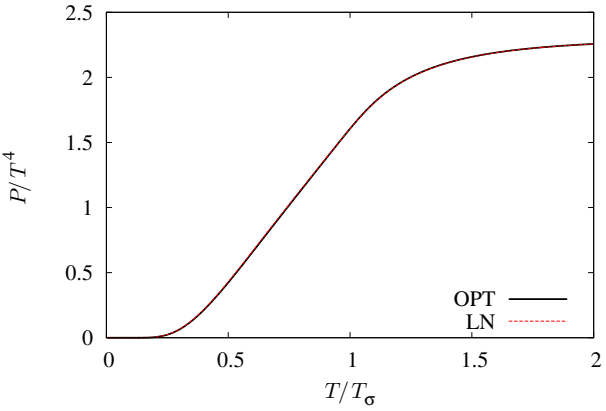

Figure 2.5.: Normalized pressure as a function of T/T_σ, at $\mu = 0$, obtained with the OPT (continuous line) and the LN approximation (dashed line)

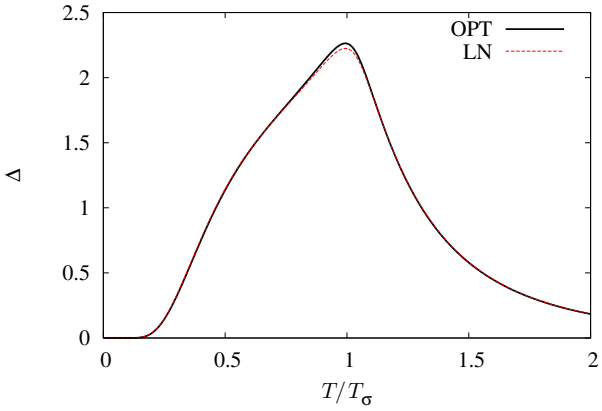

Figure 2.6.: Trace anomaly as a function of T/T_σ, at $\mu = 0$, obtained with the OPT (continuous line) and with the LN approximation (dashed line).

The number-of-particle fluctuations are characterized by the dispersion

$$\left\langle (\Delta N)^2 \right\rangle = \left\langle N^2 \right\rangle - \langle N \rangle^2 \tag{2.59}$$

for the number-of-particles operator $N = \int \psi^+(r)\psi(r)dr$ with ψ being a field operator. The average number of particles, N, is a statistical average $N = \langle N \rangle = \int \rho(r)dr$ where $\rho(r) = \left\langle \psi^+(r)\psi(r) \right\rangle$ is the density of particles. Here we keep in mind an equilibrium state, because of which $\rho(r)$ does not depend on time. But $\rho(r)$ depends on the spatial variable r, when the system is non-uniform (which is not the case under study in this work).

As discussed in Sec 1.2, to study QCD at finite densities using Monte Carlo simulations one can Taylor-expand the pressure as a power series in μ/T,

$$\frac{P}{T^4} = \sum_{n=0}^{\infty} c_{2n}(T) \left(\mu/T\right)^{2n}. \tag{2.60}$$

Note that there are only even powers of μ/T due to the reflexion symmetry, which means that the pressure is an even function with respect to μ, $P(\mu) = P(-\mu)$ [25]. The coefficients of the series (also known as cumulants) can be identified with the quark number susceptibilities.

Once the pressure has been evaluated within a given model approximation the coefficients can be obtained from

$$c_n(T) = \frac{1}{n!} \left. \frac{\partial^n P(T,\mu)/T^4}{\partial \left(\mu/T\right)^n} \right|_{\mu=0}. \tag{2.61}$$

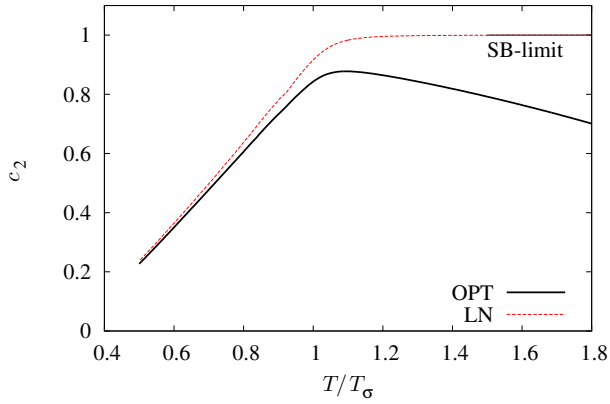

Figure 2.7.: Taylor expansion coefficient c_2 as a function of T/T_σ obtained with the OPT (continuous line) and with the LN approximation (dashed line).

Having determined some of these coefficients one can then calculate other thermodynamical quantities like the quark number density or the quark number susceptibility, which are respectively given by

$$\frac{\rho}{T^3} = \frac{\partial P\left(T,\mu\right)/T^4}{\partial\left(\mu/T\right)} = 2c_2\frac{\mu}{T} + 4c_4\left(\frac{\mu}{T}\right)^3 + \cdots, \tag{2.62}$$

$$\frac{\chi_q}{T^2} = \frac{\partial^2 P\left(T,\mu\right)/T^4}{\partial\left(\mu/T\right)^2} = 2c_2 + 12c_4\left(\frac{\mu}{T}\right)^2 + \cdots \tag{2.63}$$

Nowadays the evaluation of these cumulants is receiving a lot of attention from LQCD researchers and the considerable amount of data already available can be used to check the reliability of other non-perturbative techniques such as the OPT and the LN approximation. With this purpose, in this work we will be concerned with the evaluation of c_2. We also point out that the NJL model does not seem to produce reliable results for higher order coefficients when they are calculated taking the derivatives directly from the pressure expression. In this situation it is preferable to follow the method adopted in Ref. [57], which consists in evaluating P/T^4, at a fixed temperature and for different values of μ, then fit it (e.g., numerically) to a polynomial in μ/T.

Figure 2.7 shows the coefficient c_2 obtained with the OPT and with the LN approximation for the NJL model. We can see from the figure that the OPT does not behave as expected, since the value of c_2 is decreasing for $T > T_\sigma$ and is moving away from the Stefan–Boltzmann limit, which takes place at sufficiently high temperatures when the thermal fluctuations overcome the interparticle interactions and the system behaves as a free gas whose pressure, in the continuum limit, is given by [58]

$$\frac{P_{SB}}{T^4} = \frac{8\pi^2}{45}\left[1 + \frac{21}{32}N_f\left(1 + \frac{120}{7}\hat{\mu}^2 + \frac{240}{7}\hat{\mu}^4\right)\right]. \tag{2.64}$$

Then, using Eq. (2.61) we find the Stefan–Boltzmann limit for c_2

$$c_2^{SB} = 1. \tag{2.65}$$

At this stage it seems puzzling that the OPT, which supposedly should produce results more accurate than the LN approximation, seems to perform rather poorly at high temperatures. Moreover, none of the LQCD evaluations for this coefficient reproduce the maximum for $c_2\,(T)$ observed in the OPT results. Nevertheless, a result similar to ours has been obtained by Steinheimer and Schramm [59] who used the LN approximation to investigate the NJL model in the presence of a repulsive vector channel. In the next section we review this version of the NJL model and the LN result for the free energy in order to shed light into the OPT results.

2.4. Repulsive vector interaction in the NJL model

In the Introduction we have emphasized the importance of a vector interaction in the studies of compressed quark matter. Within the NJL model such a term can be of the form $-G_V\left(\bar{\psi}\gamma_\mu\psi\right)^2$ with $G_V > 0$ describing repulsion which is the case here and $G_V < 0$ describing attraction. Then the standard NJL lagrangian density becomes

$$\mathcal{L}_V = \bar{\psi}\left(i\partial\!\!\!/ - \hat{m}_0\right)\psi + G_S\left[\left(\bar{\psi}\psi\right)^2 + \left(\bar{\psi}i\gamma_5\boldsymbol{\tau}\psi\right)^2\right] - G_V\left(\bar{\psi}\gamma^\mu\psi\right)^2, \tag{2.66}$$

and the effective potential in the LN approximation reads [2]

$$\mathcal{F}_{LN} = \frac{\sigma^2}{4G_S} - 4G_V N_f^2 N_c^2 I_3^2\left(\tilde{\mu}, T\right) - 2N_f N_c I_1\left(\tilde{\mu}, T\right), \tag{2.67}$$

where $I_1(\tilde{\mu}, T)$ and $I_3(\tilde{\mu}, T)$ can be readily obtained from Eqs. (2.38) and (2.40) upon replacing $\mu \to \tilde{\mu} = \mu - 2G_V\rho$, with $\rho = 2N_cN_fI_3$, and $m_0 + \eta \to m_0 + \sigma$. Fukushima [20] has shown that the *combined* effect of $\tilde{\mu}$ and $-4G_VN_c^2N_f^2I_3^2$ in the above equation is to produce a *net* effect similar to $+4G_VN_c^2N_f^2I_3^2$. This interesting result allows us to better understand the type of $1/N_c$ contributions radiatively generated by the OPT. An inspection of Eq. (2.37) reveals that this approximation generates a $+4G_SN_cN_fI_3^2$ term which is similar to the $+4G_VN_c^2N_f^2I_3^2$ term appearing in the LN result.

Let us pursue this investigation by analyzing the chiral transition at high densities obtained with the OPT (at $G_V = 0$) and the LN approximation (at $G_V = 0$ and $G_V \neq 0$).

Note that, in order to obtain thermodynamical results with the LN approximation, at $G_V \neq 0$, one needs to solve the following set of equations

$$\frac{\partial\mathcal{F}}{\partial\sigma} = 0, \quad \text{and} \quad \frac{\partial\mathcal{F}}{\partial\tilde{\mu}} = 0. \tag{2.68}$$

Fig. 2.8 shows the predictions for the chiral transition at low temperatures and high

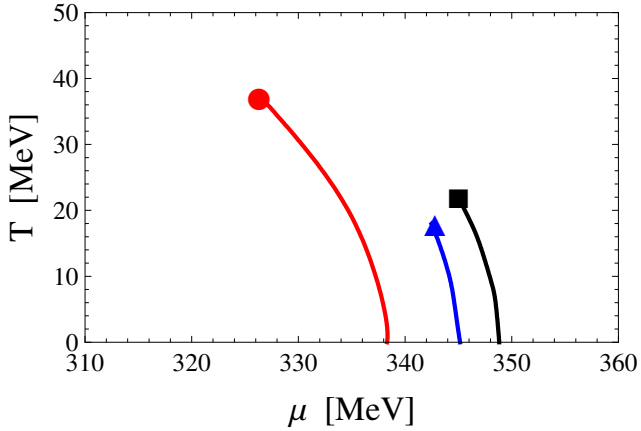

Figure 2.8.: Phase diagram in the T–μ plane for the NJL model showing the first order transition lines and the critical end points. The LN with $G_V = 0$ is denoted by the circle, the LNG_V with $G_V = G_S/(N_f N_c)$ is denoted by the triangle and the OPT is denoted by the square.

chemical potential values where the transition is of the first kind. This transition line starts at $T = 0$ and terminates at a second order transition point which defines a critical end point (when $m_0 \neq 0$) since at supercritical temperatures a crossover takes place as already discussed (note that in the chiral limit case, the first order transition line terminates at a tricritical point and at supercritical temperatures one has second order phase transitions). This low-T/high-μ portion of the QCD phase diagram is very important for astrophysical applications and the fact that the transition is of the first kind has non-negligible consequences concerning the structure of compact stellar objects. For example, within this kind of phase transition one may have two substances, with distinct densities, coexisting at the same P, T and μ. In the case of strongly interacting matter these two substances may represent hadronic and quark matter which could lead to the formation a hybrid star instead of a pure neutron star. Our results show that both, the OPT and the LN approximation with $G_V \neq 0$ (LNG_V) reduce the first order transition in relation to the LN case with $G_V = 0$. Also, for a given temperature, the coexistence chemical potential value at which the transition occurs is shifted to higher values within the OPT and the LNG_V indicating that these two different model approximations produce a similar type of physics as one could infer by comparing their free energies.

We have already emphasized the important role played by a repulsive vector channel in the description of compressed quark matter. As we have just shown the OPT seems to reproduce the same effects without the need to explicitly introduce such a term (and one more parameter!) at the tree level. In the OPT case the radiative corrections,

which are $1/N_c$ suppressed, account for a vector type of channel as a consequence of the Fierz identities which manifest themselves when exchange (two loop) diagrams are considered. So far, in view of our comparisons between this method, the LN and the LNG_V, one may say that at least for temperatures not much higher than the one which signals the chiral transition the OPT represents an improvement over the LN (at $G_V = 0$). So, the OPT can be seen as a powerful alternative to investigate the low-T/high-μ part of the QCD phase diagram which is currently non-accessible to the LQCD simulations. However, our evaluation of the important c_2 cumulant has revealed that at temperatures higher than T_c the OPT presents a problem similar to the one detected within the LNG_V approximation: the failure to attain the SB limit! Steinheimer and Schramm, who employed the LNG_V, concluded that G_V should drop to zero after T_c so that the SB limit at high T while reproducing the correct physics at $T < T_c$. We will discuss this conjecture with more detail at the end of Chap. 4.

3. The Polyakov–Nambu–Jona-Lasinio Model

The standard version of the NJL does not incorporate confinement and therefore is of limited interest if one aims to perform a realistic description of QCD. In this case, it becomes mandatory to find some way of simulating confinement within the original model. With this purpose, in Ref. [5] the *Polyakov loop* has been added to the NJL Lagrangian to produce the Polyakov-loop-extended NJL model (PNJL)

$$\mathcal{L}_{PNJL} = \bar{\psi}\left(i\not{D} - \hat{m}_0\right)\psi + G_S\left[\left(\bar{\psi}\psi\right)^2 + \left(\bar{\psi}i\gamma_5\boldsymbol{\tau}\psi\right)^2\right] - \mathcal{U}\left(l, l^*, T\right), \tag{3.1}$$

where the covariant derivative is given by

$$D^\mu = \partial^\mu - iA^\mu \quad \text{with} \quad A^\mu = \delta^0_\mu A^0, \tag{3.2}$$

with the $SU(N)$ gauge coupling constant, g, absorbed in $A^\mu\left(x\right) = g\mathcal{A}^\mu_a\left(x\right)\dfrac{\lambda_a}{2}$, where $\mathcal{A}^\mu_a\left(x\right)$ is the $SU\left(3\right)$ gauge field and λ_a represent the Gell-Mann matrices [60].

Before presenting the Polyakov potential $\mathcal{U}\left(l, l^*, T\right)$ let us now define the Wilson line which winds once through a periodic time direction [61–63]

$$L\left(\boldsymbol{x}\right) \equiv \mathcal{P}\exp\left[i\int_0^\beta d\tau A_4\left(\tau, \boldsymbol{x}\right)\right], \tag{3.3}$$

where $\beta = 1/T$ and $A_4 = iA_0$ is the temporal component of the Euclidean gauge field $(A_4, \boldsymbol{A})$. In the same expression, $\mathcal{P}$ denotes the time ordering operator, which indicates that the integral must be calculated ordering the time variable τ as [30]

$$\mathcal{P}\left[A_4\left(\tau_1, \boldsymbol{x}\right)A_4\left(\tau_2, \boldsymbol{x}\right)\right] = \begin{cases} A_4\left(\tau_1, \boldsymbol{x}\right)A_4\left(\tau_2, \boldsymbol{x}\right) & \text{if} \quad \tau_1 > \tau_2 \\ A_4\left(\tau_2, \boldsymbol{x}\right)A_4\left(\tau_1, \boldsymbol{x}\right) & \text{if} \quad \tau_2 > \tau_1 \end{cases}. \tag{3.4}$$

The expectation value of the Polyakov loop Φ is then given by [32]

$$\Phi \equiv \left\langle l\left(\boldsymbol{x}\right)\right\rangle, \quad \text{and} \quad \bar{\Phi} \equiv \left\langle l^*\left(\boldsymbol{x}\right)\right\rangle, \tag{3.5}$$

where

$$l\left(\boldsymbol{x}\right) \equiv \frac{1}{N_c}\mathrm{Tr}L\left(\boldsymbol{x}\right) \tag{3.6}$$

is the traced Polyakov loop.

Finally, the potential $\mathcal{U}\left(l, l^*, T\right)$ is fixed by comparison with pure-gauge lattice QCD [64], from which one obtains the following ansatz [62],

$$\frac{\mathcal{U}\left(l, l^*, T\right)}{T^4} = -\frac{1}{2}b_2\left(T\right)ll^* + b_4\left(T\right)\ln\left[1 - 6ll^* + 4\left(l^3 + {l^*}^3\right) - 3\left(ll^*\right)^2\right], \tag{3.7}$$

with

$$b_2(T) = a_0 + a_1\left(\frac{T_0}{T}\right) + a_2\left(\frac{T_0}{T}\right)^2, \quad b_4(T) = b_4\left(\frac{T_0}{T}\right)^3. \tag{3.8}$$

The parameters a_i, b_i, taken from Ref. [62] are listed in table 3.1, where T_0 is the critical temperature for deconfinement in the pure-gauge sector whose value is fixed at 270 MeV.

a_0	a_1	a_2	b_4
3.51	-2.47	15.22	-1.75

Table 3.1.: Parameter set use for the Polyakov loop potential

3.1. Center symmetry group $Z(3)$

By construction, QCD is invariant under local gauge transformations of the $SU(N_c)$ group and, as a consequence, it is also invariant under the subgroups of $SU(N_c)$ such as the center group $Z(N_c)$, that is related to confinement. The center group, which is composed by elements that commute with all the other elements of $SU(N_c)$ [31, 32, 65], has the elements

$$z_n = \mathbf{1}\exp\left(\frac{2\pi i n}{N_c}\right) \quad (n = 0, 1, 2, \cdots, N_c - 1). \tag{3.9}$$

In our case, $N_c = 3$, so that the center group is $Z(3)$, which is composed by tree elements. Since the center group has a finite number of elements the group of transformations cannot change continuously from point to point, thus it is a global symmetry of the QCD Lagrangian in the pure gauge sector.

In QCD the following periodic conditions for quarks and gluons holds:

$$\psi(0, \boldsymbol{x}) = -\psi(\beta, \boldsymbol{x}) \quad \text{and} \quad A_\mu(0, \boldsymbol{x}) = A_\mu(\beta, \boldsymbol{x}). \tag{3.10}$$

Let us now investigate what happens to the boundary conditions under local $SU(3)$ transformations:

$$\begin{aligned} \psi(0, \boldsymbol{x}) &\to U(0, \boldsymbol{x})\,\psi(0, \boldsymbol{x}), \\ \psi(\beta, \boldsymbol{x}) &\to U(\beta, \boldsymbol{x})\,\psi(\beta, \boldsymbol{x}), \end{aligned} \tag{3.11}$$

$$\begin{aligned} A_\mu(0, \boldsymbol{x}) &\to U(0, \boldsymbol{x})\,A_\mu(0, \boldsymbol{x})\,U^\dagger(0, \boldsymbol{x}) - \frac{1}{ig}U(0, \boldsymbol{x})\,\partial_\mu U^\dagger(0, \boldsymbol{x}), \\ A_\mu(\beta, \boldsymbol{x}) &\to U(\beta, \boldsymbol{x})\,A_\mu(\beta, \boldsymbol{x})\,U^\dagger(\beta, \boldsymbol{x}) - \frac{1}{ig}U(\beta, \boldsymbol{x})\,\partial_\mu U^\dagger(\beta, \boldsymbol{x}), \end{aligned} \tag{3.12}$$

noting that, in order to preserve the boundary conditions for quarks, the $SU(3)$ transformations must be periodic

$$U(0,\boldsymbol{x}) = U(\beta,\boldsymbol{x}). \tag{3.13}$$

However, gluons are adjoint fields and their transformations involve the inverse of the transformation matrix, which means that only transformation matrices that commute with the gluon field will keep it unchanged. So, these elements are the elements of the $Z(3)$ symmetry group, meaning that

$$U(0,\boldsymbol{x}) = zU(\beta,\boldsymbol{x}). \tag{3.14}$$

It is important to note that the $Z(3)$ symmetry arising from the boundary conditions are not the same as the symmetry of the Lagrangian where the fields are rotated by the same element of $Z(3)$ at every point. On the other hand, in the boundary conditions, the rotations of the gluon fields is only at $\tau = \beta$. In other words, the QCD Lagrangian density is invariant under general gauge transformations 3.12, but the boundary condition may not be respect.

Within gauge transformations the Wilson line transforms as

$$L(\boldsymbol{x}) \to U(\beta)\, L(\boldsymbol{x})\, U^{\dagger}(\beta), \tag{3.15}$$

so that transformations such as the one described by Eq. (3.14) lead to

$$l(\boldsymbol{x}) \to z l(\boldsymbol{x}), \tag{3.16}$$

owing the fact that the trace of $L(\boldsymbol{x})$ is invariant under gauge transformations. Then, the expectation value of the Polyakov loop (Φ) must be zero relating the $Z(3)$ symmetry with confinement, where $\Phi = 0$ represents the confined phase whilst the deconfined phase is accompanied by the spontaneous breaking of the center symmetry. In order to visualize this we offer Fig. 3.1 which displays the thermodynamical potential in the pure gauge sector, where quarks are not taken into account. The figure clearly shows that at temperatures below the critical temperature, T_0, a global minimum arises at $\Phi = 0$, signaling the confined phase. On the other hand, when the temperature is greater than T_0, the center symmetry is spontaneously broken, and now there are three minima which correspond to a deconfined phase, when the confinement order parameter acquires a finite value $(\Phi \neq 0)$.

In the presence of dynamical quarks the $Z(3)$ symmetry is explicitly broken and one cannot rigorously talk of a phase transition. Nevertheless, the expectation value of the Polyakov loop serves as an indicator of the crossover between the phase of color confinement $(\Phi \to 0)$ and the one where color is deconfined $(\Phi \to 1)$.

A physical interpretation of Φ is related to the single quark free energy $f_q(\boldsymbol{x})$ by

$$f_q = -T \ln\left(\langle l(\boldsymbol{x})\rangle\right), \tag{3.17}$$

and for a static quark anti-quark pair, it can be written as the correlation of two Polyakov loops

$$f_q(\boldsymbol{x}-\boldsymbol{y}) = -T \ln\left(\left\langle l(\boldsymbol{y})^{\dagger}\, l(\boldsymbol{x})\right\rangle\right). \tag{3.18}$$

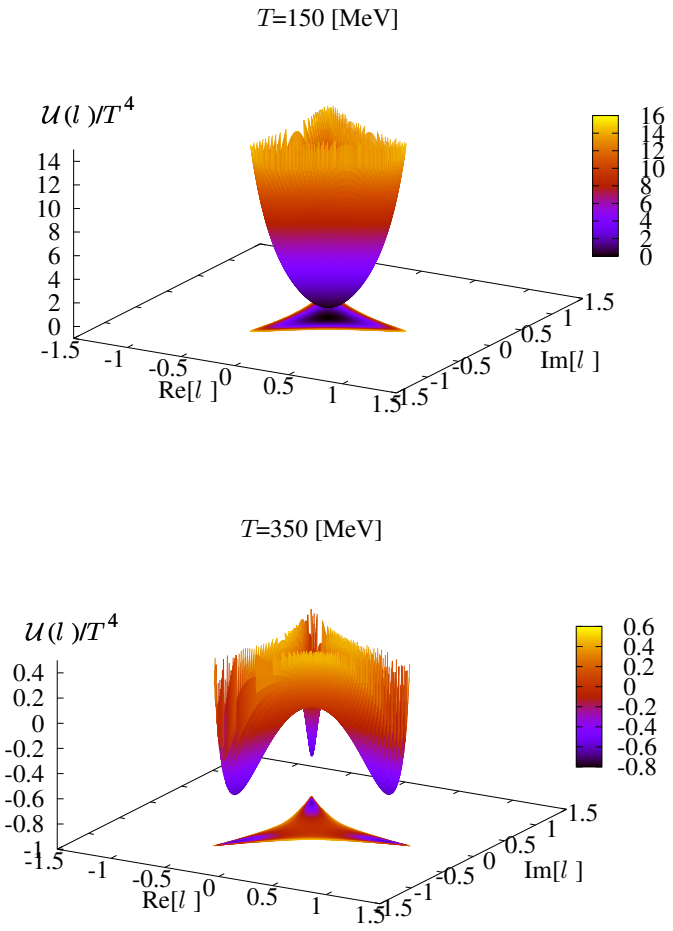

Figure 3.1.: Effective potential in the pure gauge sector for two temperatures, below and above the critical temperature T_0.

If the expectation value of the Polyakov loop is zero, that implies an infinite free energy for a single quark, or an infinite pair potential in the quark anti-quark case. This implies quark confinement justifying that the Polyakov loop be considered the order parameter for confinement.

3.2. The PNJL free energy beyond the large-N_c limit

In order to find the expression for the PNJL free energy using the OPT, we will follow exactly the procedure adopted in Sec. 2.2, but now, instead of $\not{\phi}$ we have $\not{\mathcal{D}}$, and also the additional potential $\mathcal{U}\left(\Phi,\bar{\Phi},T\right)$ in the Lagrangian. Technically the major difference is that within the PNJL model the trace over color space must be carried out after the sums over Matsubara's frequencies have been performed. Let us start by adapting Eq. (2.31) to the PNJL case. Setting $n_\pi = 3$, $\boldsymbol{\nu} = 0$ and $\alpha = \eta$ yields

$$\begin{aligned}
\mathcal{F} = {} & \mathcal{U}\left(l,l^*,T\right) + \frac{N_c\sigma^2}{2\lambda} + 2iN_f\int\frac{d^4p}{(2\pi)^4}\mathrm{Tr_c}\ln\left[-p^2+(\eta-m_0)^2\right] \\
& + 4i\delta N_f\int\frac{d^4p}{(2\pi)^4}\mathrm{Tr_c}\frac{(\eta+m_0)(\eta-\sigma)}{-p^2+(\eta+m_0)^2} \\
& - 8\delta\frac{\lambda N_f}{N_c}\int\frac{d^4p}{(2\pi)^4}\frac{d^4q}{(2\pi)^4}\mathrm{Tr_c}\frac{p_0}{-p^2+(\eta+m_0)^2}\frac{q_0}{-q^2+(\eta+m_0)^2} \\
& + 4\delta\frac{\lambda N_f}{N_c}(\eta+m_0)^2\int\frac{d^4p}{(2\pi)^4}\frac{d^4q}{(2\pi)^4}\mathrm{Tr_c}\frac{1}{-p^2+(\eta+m_0)^2}\frac{1}{-q^2+(\eta+m_0)^2}, \qquad (3.19)
\end{aligned}$$

where now, $p_0 \to i\omega_n + \mu - iA_4$. Denoting $\mu' = \mu - iA_4$ and introducing the usual Matsubara's sum we get

$$\begin{aligned}
\mathcal{F} = {} & \mathcal{U}\left(l,l^*,T\right) + \frac{N_c\sigma^2}{2\lambda} - \frac{2N_f}{\beta}\int\frac{d^3p}{(2\pi)^3}\mathrm{Tr_c}\sum_{n=-\infty}^{\infty}\ln\left[\left(\omega_n - i\mu'\right)^2 + E_p^2\right] \\
& - \delta\frac{4Nf}{\beta}(\eta+m_0)(\eta-\sigma)\int\frac{d^3p}{(2\pi)^3}\mathrm{Tr_c}\sum_{n=-\infty}^{\infty}\frac{1}{\left(\omega_n - i\mu'\right)^2 + E_p^2} \\
& - 8\delta\frac{\lambda N_f}{\beta^2 N_c}\int\frac{d^3p}{(2\pi)^3}\frac{d^3p}{(2\pi)^3}\mathrm{Tr_c}\sum_{n=-\infty}^{\infty}\sum_{m=-\infty}^{\infty}\frac{\omega_n - i\mu'}{\left(\omega_n - i\mu'\right)^2 + E_p^2}\frac{\omega_m - i\mu'}{\left(\omega_m - i\mu'\right)^2 + E_q^2} \\
& - 4\delta\frac{\lambda N_f}{\beta^2 N_c}(\eta+m_0)^2\int\frac{d^3p}{(2\pi)^3}\frac{d^3p}{(2\pi)^3}\mathrm{Tr_c}\sum_{n=-\infty}^{\infty}\sum_{m=-\infty}^{\infty}\frac{1}{\left(\omega_n + i\mu'\right)^2 + E_p^2} \\
& \times \frac{1}{\left(\omega_m + i\mu'\right)^2 + E_q^2}, \qquad (3.20)
\end{aligned}$$

where the notation $\mathrm{Tr_c}$ is a reminder that the traces over color space have not yet been performed. To our knowledge this evaluation has not been performed before

for the two loop contributions represented by the two last terms of Eq. (3.20). This straightforward but lengthly exercise is presented in Appendix C. Then, upon replacing $\lambda \to 2G_S N_c$ and setting $\delta = 1$ one obtains

$$\begin{aligned}\mathcal{F}(\eta,\sigma,l,l^*,\mu,T) =& \mathcal{U}(l,l^*,T) + \frac{\sigma^2}{4G_S} - 2N_f I_1(\mu,T) + 2N_f N_c(\eta+m_0)(\eta-\sigma) I_2(\mu,T) \\ &+ 4G_S N_f N_c\left[I_3^2(\mu,T) + \Delta I_3^2(\mu,T)\right] \\ &- 2G_S N_f N_c(\eta+m_0)^2\left[I_2^2(\mu,T) + \Delta I_2^2(\mu,T)\right], \end{aligned} \tag{3.21}$$

where

$$I_1(\mu,T) = \int \frac{d^3p}{(2\pi)^3}\left\{N_c E_p + \ln\left[g_l^+(E_p)\right] + \ln\left[g_l^-(E_p)\right]\right\}, \tag{3.22}$$

$$I_2(\mu,T) = \int \frac{d^3p}{(2\pi)^3}\frac{1}{E_p}\left[1 - f_l^+ - f_l^-\right], \tag{3.23}$$

$$I_3(\mu,T) = \int \frac{d^3p}{(2\pi)^3}\left[f_l^+ - f_l^-\right] \tag{3.24}$$

and

$$f_l^+(E_p) = \frac{l e^{-\beta(E_p-\mu)} + 2l^* e^{-2\beta(E_p-\mu)} + e^{-3\beta(E_p-\mu)}}{g_l^+(E_p)}, \tag{3.25}$$

$$f_l^-(E_p) = \frac{l^* e^{-\beta(E_p+\mu)} + 2l e^{-2\beta(E_p+\mu)} + e^{-3\beta(E_p+\mu)}}{g_l^-(E_p)}, \tag{3.26}$$

$$g_l^+(E_p) = 1 + 3l e^{-\beta(E_p-\mu)} + 3l^* e^{-2\beta(E_p-\mu)} + e^{-3\beta(E_p-\mu)}, \tag{3.27}$$

$$g_l^-(E_p) = 1 + 3l^* e^{-\beta(E_p+\mu)} + 3l e^{-2\beta(E_p+\mu)} + e^{-3\beta(E_p+\mu)}. \tag{3.28}$$

The integrals $\Delta I_2^2(\mu,T)$ and $\Delta I_3^2(\mu,T)$ are given by

$$\Delta I_3^2(\mu,T) = \int \frac{d^3p}{(2\pi)^3}\frac{d^3q}{(2\pi)^3}\Delta_3^2, \tag{3.29}$$

and

$$\Delta I_2^2(\mu,T) = \int \frac{d^3p}{(2\pi)^3}\frac{d^3q}{(2\pi)^3}\Delta_2^2, \tag{3.30}$$

where

$$\begin{aligned}
\Delta_2^2 = & \frac{e^{-\beta\left(E_p-\mu\right)}e^{-\beta\left(E_q-\mu\right)}}{g_l^+(E_p)g_l^+(E_q)}\left\{2\left(l^2-l^*\right)+\left(ll^*-1\right)\left[e^{-\beta\left(E_p-\mu\right)}+e^{-\beta\left(E_q-\mu\right)}\right]\right. \\
& \left.+\,2\left(l^{*2}-l\right)e^{-\beta\left(E_p-\mu\right)}e^{-\beta\left(E_q-\mu\right)}\right\} \\
& +\frac{e^{-\beta\left(E_p-\mu\right)}e^{-\beta\left(E_q+\mu\right)}}{g_l^+(E_p)g_l^-(E_q)}\left\{2\left(l-l^{*2}\right)e^{-\beta\left(E_p-\mu\right)}+2\left(l^*-l^2\right)e^{-\beta\left(E_q+\mu\right)}\right. \\
& \left.+\,\left(1-ll^*\right)\left[1+e^{-\beta\left(E_p-\mu\right)}e^{-\beta\left(E_q+\mu\right)}\right]\right\} \\
& +\frac{e^{-\beta\left(E_q-\mu\right)}e^{-\beta\left(E_p+\mu\right)}}{g_l^+(E_q)g_l^-(E_p)}\left\{2\left(l-l^{*2}\right)e^{-\beta\left(E_q-\mu\right)}+2\left(l^*-l^2\right)e^{-\beta\left(E_p+\mu\right)}\right. \\
& \left.+\,\left(1-ll^*\right)\left[1+e^{-\beta\left(E_q-\mu\right)}e^{-\beta\left(E_p+\mu\right)}\right]\right\} \\
& +\frac{e^{-\beta\left(E_p+\mu\right)}e^{-\beta\left(E_q+\mu\right)}}{g_l^-(E_p)g_l^-(E_q)}\left\{2\left(l^{*2}-l\right)+\left(ll^*-1\right)\left[e^{-\beta\left(E_p+\mu\right)}+e^{-\beta\left(E_q+\mu\right)}\right]\right. \\
& \left.+\,2\left(l^2-l^*\right)e^{-\beta\left(E_p+\mu\right)}e^{-\beta\left(E_q+\mu\right)}\right\}, \qquad (3.31)
\end{aligned}$$

and

$$\begin{aligned}
\Delta_3^2 = & \frac{e^{-\beta\left(E_p-\mu\right)}e^{-\beta\left(E_q-\mu\right)}}{g_l^+(E_p)g_l^+(E_q)}\left\{2\left(l^2-l^*\right)+\left(ll^*-1\right)\left[e^{-\beta\left(E_p-\mu\right)}+e^{-\beta\left(E_q-\mu\right)}\right]\right. \\
& \left.+\,2\left(l^{*2}-l\right)e^{-\beta\left(E_p-\mu\right)}e^{-\beta\left(E_q-\mu\right)}\right\} \\
& -\frac{e^{-\beta\left(E_p-\mu\right)}e^{-\beta\left(E_q+\mu\right)}}{g_l^+(E_p)g_l^-(E_q)}\left\{2\left(l-l^{*2}\right)e^{-\beta\left(E_p-\mu\right)}+2\left(l^*-l^2\right)e^{-\beta\left(E_q+\mu\right)}\right. \\
& \left.+\,\left(1-ll^*\right)\left[1+e^{-\beta\left(E_p-\mu\right)}e^{-\beta\left(E_q+\mu\right)}\right]\right\} \\
& -\frac{e^{-\beta\left(E_q-\mu\right)}e^{-\beta\left(E_p+\mu\right)}}{g_l^+(E_q)g_l^-(E_p)}\left\{2\left(l-l^{*2}\right)e^{-\beta\left(E_q-\mu\right)}+2\left(l^*-l^2\right)e^{-\beta\left(E_p+\mu\right)}\right. \\
& \left.+\,\left(1-ll^*\right)\left[1+e^{-\beta\left(E_q-\mu\right)}e^{-\beta\left(E_p+\mu\right)}\right]\right\} \\
& +\frac{e^{-\beta\left(E_p+\mu\right)}e^{-\beta\left(E_q+\mu\right)}}{g_l^-(E_p)g_l^-(E_q)}\left\{2\left(l^{*2}-l\right)+\left(ll^*-1\right)\left[e^{-\beta\left(E_p+\mu\right)}+e^{-\beta\left(E_q+\mu\right)}\right]\right. \\
& \left.+\,2\left(l^2-l^*\right)e^{-\beta\left(E_p+\mu\right)}e^{-\beta\left(E_q+\mu\right)}\right\}. \qquad (3.32)
\end{aligned}$$

Note that, when $\Phi \to 1$, and, $\bar{\Phi} \to 1$, we have $\Delta_2^2 = 0$ and $\Delta_3^2 = 0$. Furthermore, in this case, the expressions for I_1, I_2 and I_3 become identical to the ones used in the standard NJL model. In other words, in the high temperature limit the PNJL model and the NJL model are, when the deconfined phase has been reached, equivalent.

For comparison purposes it is convenient to present the PNJL free energy ontained with the LN approximation which is given by

$$\mathcal{F}_{LN}\left(\sigma, l, l^{*}, \mu, T\right) = \mathcal{U}\left(l, l^{*}, T\right) + \frac{\sigma^{2}}{4G_{S}} - 2N_{f} I_{1}\left(\mu, T\right), \tag{3.33}$$

where $I_1(\mu, T)$ is given by Eq. (3.22) (with the obvious replacement $\eta \to \sigma$).

In order to obtain thermodynamical quantities from the OPT free energy one must then solve the following set of coupled equations.

$$\frac{\partial \mathcal{F}}{\partial \eta} = 0, \quad \frac{\partial \mathcal{F}}{\partial \sigma} = 0, \quad \frac{\partial \mathcal{F}}{\partial} = 0, \quad \frac{\partial \mathcal{F}}{\partial^{*}} = 0. \tag{3.34}$$

Then, the OPT pressure for the PNJL case is simply

$$P = -\mathcal{F}\left(\bar{\eta}, \bar{\sigma}, \Phi, \bar{\Phi}, \mu, T\right). \tag{3.35}$$

Except for the PMS equation (first relation in Eqs. (3.34)) the same sort of manipulation is also needed when the LN approximation is used.

3.3. Numerical results at finite temperature and zero chemical potential

Let us now compare the OPT, the LN and the LQCD results at $\mu = 0$ when $\Phi = \bar{\Phi}$ [28] yielding a simpler set of coupled equations.

The PNJL model has two order parameters and the system suffers two transitions; one from a non-chirally symmetric phase to an approximately chiral phase and another from a confined to a deconfined phase. In principle these two different transitions could occur at different critical temperatures but LQCD simulations show that in fact they coincide at $\mu = 0$. As can be seen in Fig. 3.2, the predicted critical temperature for deconfinement (T_Φ) is almost the same for OPT and for the LN approximation ($\Delta T_\Phi \simeq 1$ MeV), while the critical temperature for the chiral transition (T_σ) presents a bigger difference ($\Delta T_\sigma \simeq 5$ MeV). Furthermore, the predicted critical temperature for the chiral transition is larger than the critical temperature for deconfinement in both approximations.

Table 3.2.: Critical temperatures for the chiral (T_σ) and the deconfinement (T_Φ) transitions obtained with the OPT and with the LN approximation at $\mu = 0$.

	T_σ [MeV]	T_Φ [MeV]
OPT	217	213
LN	222	214

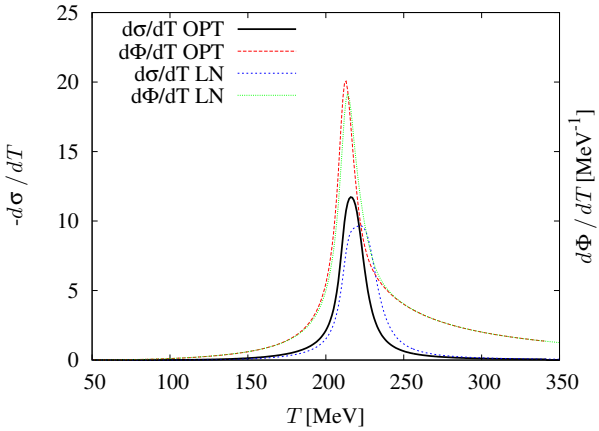

Figure 3.2.: Thermal susceptibilities, $-d\bar{\sigma}/dT$ and $d\Phi/dT$, as functions of the temperature obtained with the OPT and with the LN approximation.

Table 3.2 shows the critical temperatures for the chiral and the deconfinement transitions calculated with the OPT and the LN approximation and Fig. 3.3 displays the effective mass as a function of T/T_σ. We can note that the PNJL model presents a sharper transition than the NJL model highlighting the confinement effect of the Polyakov loop. The effective mass remains almost constant until it reaches the pseudocritical temperature, T_σ, and then falls rapidly to the current mass value, m_0, while in the NJL model the transition is more gradual. This means that the crossover region is sharper within the PNJL than within the standard version.

The deconfinement order parameter, Φ, evaluated with both approximations does not present a noticeable difference at $\mu = 0$ as can be seen in Fig. 3.4. This is not an unexpected result since the additional $1/N_c$ contributions furnished by the OPT are not much relevant at vanishing densities. In order to see that, let us consider other quantities such as the pressure which is displayed in Fig. 3.5. Again, it is clear how the Polyakov loop influences the transition by allowing the pressure to remain low until the pseudocritical temperature is reached. After that, the increase of P with T is much more dramatic within the PNJL version of the model. Then, the Polyakov loop simulates very well the effect of gluons, which are not present in the NJL type models.

Figure 3.6 shows the trace anomaly (or interacting measure) (Eq. (2.53)) as a function of T/T_σ obtained with the PNJL model and with the standard version. Once again one may observe how the Polyakov loop influences the thermal behavior, especially near the transition point. Note that the difference between the OPT and the LN is accentuated in the presence of the Φ field.

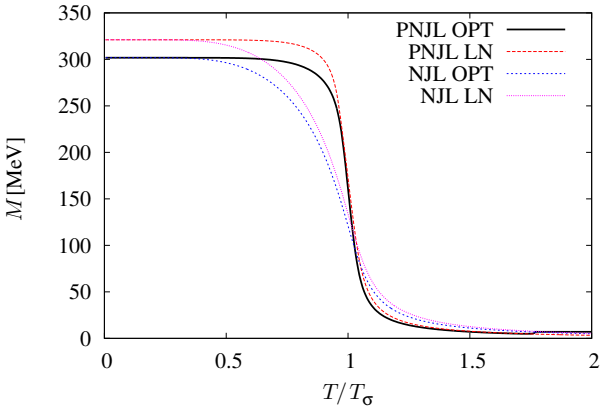

Figure 3.3.: The effective mass, M, as a function of T/T_σ, at $\mu = 0$, obtained with the OPT and with the LN approximation for the PNJL and the NJL models.

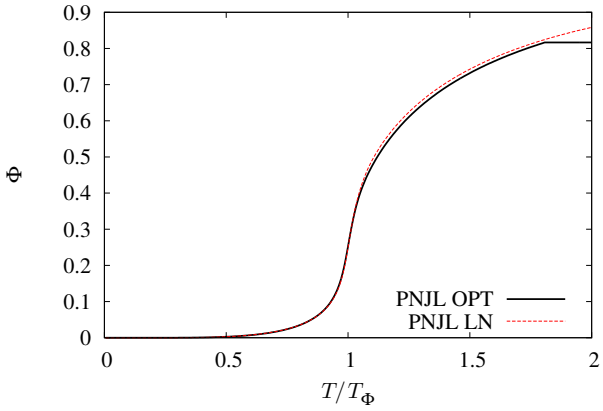

Figure 3.4.: Thermal behavior of the confinement order parameter, Φ, at $\mu = 0$, as predicted by the OPT and by the LN approximation..

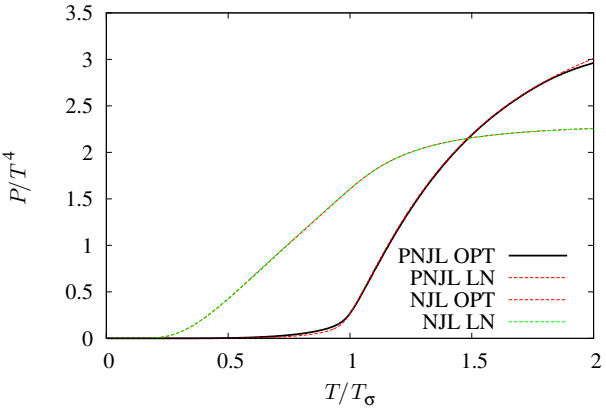

Figure 3.5.: Normalized pressure as a function of T/T_σ, at $\mu = 0$, obtained with the OPT and with the LN approximation for the PNJL and the NJL models.

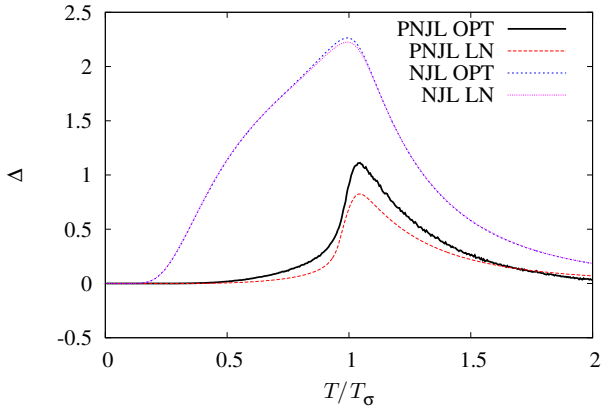

Figure 3.6.: Trace anomaly as a function of T/T_σ, at $\mu = 0$, obtained with the OPT and the LN approximation for the PNJL and the NJL models.

3.3.1. Evaluation of the second cumulant

Let us now compare the coefficient c_2 with the LQCD results given in Ref. [66], where the simulations were carried out on a 4×16^3 lattice with a two-flavor clover-improved Wilson action, with $m_\rho = 700$ MeV and $m_\pi = 505$ MeV (which is much higher than the actual physical value, $m_\pi = 135$ MeV). Then, in order to compare our results with this LQCD simulation we need to tune the current quark mass, m_0, using, as phenomenological inputs, $f_\pi \simeq 92.4$ MeV, $-\langle\bar{\psi}\psi\rangle^{1/3} \simeq 242$ MeV and $m_\pi \simeq 500$ MeV, setting $m_0 = 72.3$ MeV as the OPT value. For the LN approximation we take the parameter values adopted in Ref. [67] except for the current mass and T_0 that is kept at 270 MeV (as in the OPT case). The new parameters and the corresponding pseudocritical temperatures are listed in table 3.3. Note that for these elevated quark current masses the pseudocritical temperatures T_σ and T_Φ nearly coincide.

Table 3.3.: Parameter sets for the OPT and for the LN approximation when $m_\pi \simeq 500$ MeV

	Λ [MeV]	m_0 [MeV]	$G_S\Lambda^2$	T_σ [MeV]	T_Φ [MeV]
OPT	590	72.3	1.91	221	220
LN	631.5	72	2.19	225	224

Figure 3.7 shows c_2 as a function of T/T_σ obtained with the OPT and with the LN approximation (at $G_V = 0$ and $G_V = G_S/(N_f N_c)$) compared with LQCD data. It is evident that the inclusion of confinement was necessary in order to make the NJL model predictions more realistic. The OPT result is in excellent agreement with the LQCD data for $T/T_\sigma < 1.2$. However, at higher T, the OPT continues to deviate from the Stefan–Boltzmann limit as well as from LQCD data. Incidentally, this kind of behavior in the PNJL model augmented with a vector repulsive interaction has been reported by Steinheimer and Schramm [59, 68] within the LN framework as we have already remarked. These authors discuss the possible value of the vector repulsive coupling constant, G_V, as well as the behavior of it at $T > T_\sigma$ suggesting that G_V must be turned off for $T > T_\sigma$ so that one should expect a strong vector repulsion in the hadronic phase and a near-zero repulsion in the deconfined phase. On the other hand, the OPT finite N_c corrections generate a vector repulsive type of term *without* the additional coupling G_V. Then, one cannot use the same argument to explain the observed discrepancy. This hints that the problem could be related to fact that these effective models do not include asymptotic freedom, which is an important QCD feature. Within this fundamental theory the strong coupling runs with T decreasing as higher temperatures are considered while within the NJL models the coupling is constant. This important topic will be properly addressed in the next chapter where the entangled version of the PNJL will be considered in detail. Before doing that let us examine the case of finite temperatures and densities.

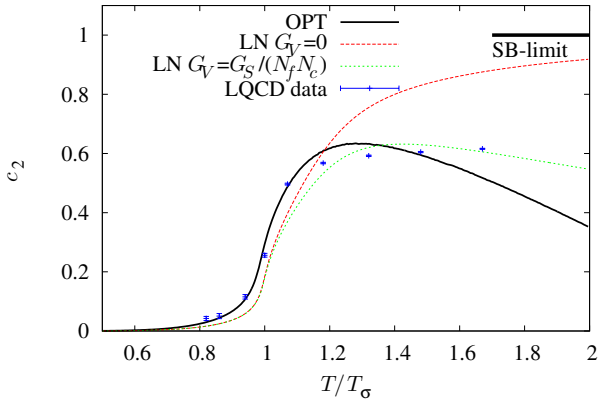

Figure 3.7.: Taylor expansion coefficient, c_2, at $\mu = 0$ as a function of T/T_σ, obtained with the OPT and with the LN approximation with $G_V = 0$ and $G_V = G_S/(N_f N_c)$ for the PNJL model. The LQCD data were taken from Ref. [66].

3.4. Results for hot and dense quark matter

At finite chemical potential the fields Φ and $\bar{\Phi}$ are no longer equal, and it may be instructive to examine their behavior. In Fig. 3.8 the expectation value of the Polyakov loop, Φ, and its conjugate, $\bar{\Phi}$, are presented as functions of the chemical potential at constant temperature and as functions of temperature at constant chemical potential within the OPT and the LN frameworks. For a given temperature value, the fields Φ and $\bar{\Phi}$ grow with μ, and this growth is more pronounced when higher temperature values are considered. The difference between the OPT and the LN approximation is accentuated at high chemical potential values as expected. On the other hand, at a fixed μ values, we note that Φ and $\bar{\Phi}$ start to grow at a lower temperature when μ is higher. Another important aspect is that in the constant T case, the difference between Φ and $\bar{\Phi}$ is larger for higher μ values within the LN approximation, while the difference decreases within the OPT. Also, in the constant μ case, both approximations predict that the difference between Φ and $\bar{\Phi}$ is higher in the confined phase. In this case, the OPT results show that the difference between Φ and $\bar{\Phi}$ is smaller than in the LN approximation as Fig. 3.9 shows.

Finally, Figs. 3.10 and 3.11 show the quark number density (ρ) and the quark number susceptibility (χ_q) respectively as functions of T/T_σ for different chemical potential values. The OPT results for ρ show a better agreement in the temperature range considered. Note also that the LN results worsen as higher values of μ are considered which hints to the importance of a repulsive vector channel in the evaluation

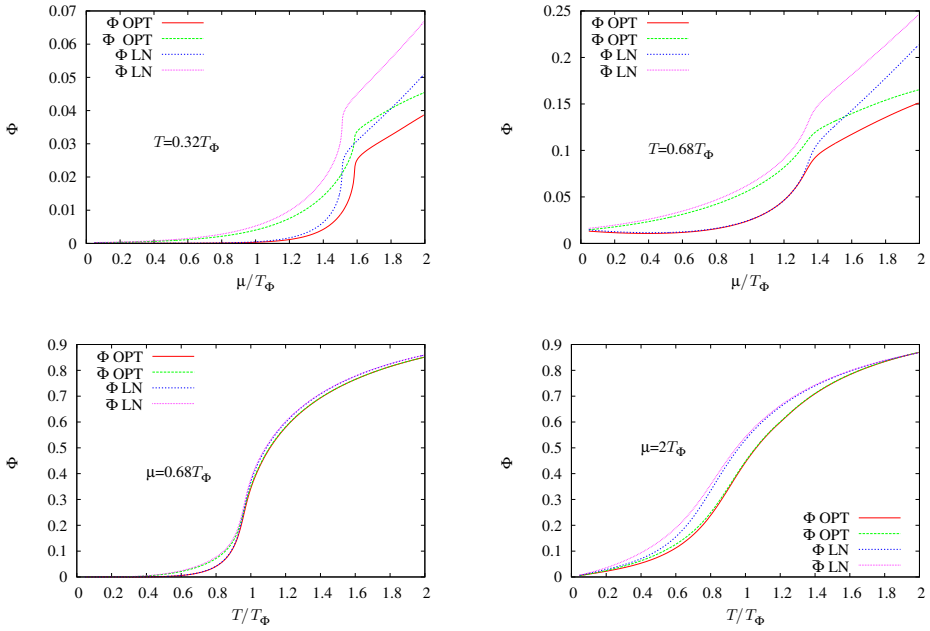

Figure 3.8.: Examples of the Polyakov loop expectation values Φ, and its conjugate $\bar{\Phi}$, obtained with the OPT and the LN approximation. In the top panels, Φ and $\bar{\Phi}$ are plotted as functions of μ/T_c at constant temperature values. In the bottom panels, Φ and $\bar{\Phi}$ are plotted as functions of T/T_Φ at constant chemical potential values.

of the quark number density. The situation gets reversed as far as the predictions for χ_q are concerned and the LN approximation performs better while the OPT results for $T > 1.2T_\sigma$ seem wrong even from a qualitative point of view. As in the evaluation of c_2, which is in fact related to χ_q at $\mu = 0$, the OPT predictions present a maximum at about $T/T_\sigma \simeq 1.2$ which is absent in the LQCD results. In the next chapter we will discuss how this situation may be eventually reversed by taking the coupling to be temperature dependent.

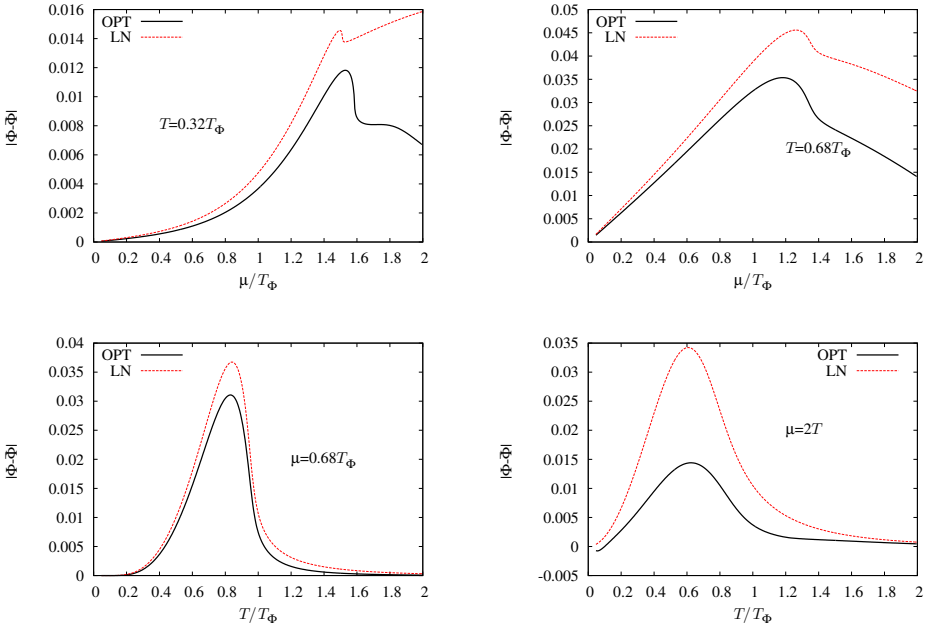

Figure 3.9.: Examples of the difference between the Polyakov loop expectation values $\left|\Phi - \bar{\Phi}\right|$ obtained with the OPT and the LN approximation. In the top panels, $\left|\Phi - \bar{\Phi}\right|$ is plotted as a function of μ/T_c at constant temperature values. In the bottom panels, $\left|\Phi - \bar{\Phi}\right|$ is plotted as a function of T/T_Φ at constant chemical potential values.

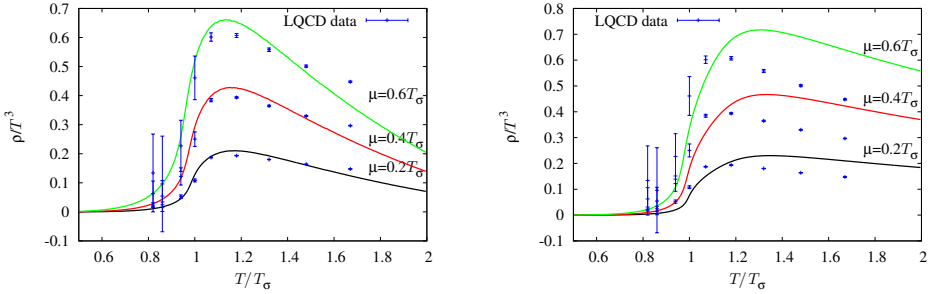

Figure 3.10.: Normalized quark number density as a function of T/T_σ for different values of μ as predicted by the OPT (left panel) and the LN approximation (right panel). The lattice data were taken from Ref. [66].

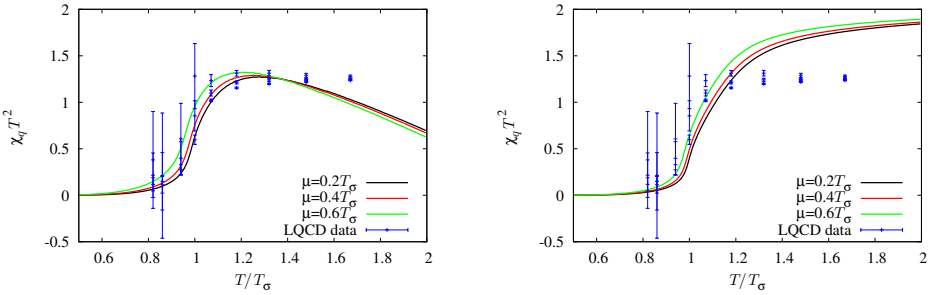

Figure 3.11.: Quark number susceptibility as a function of T/T_σ for different values of μ in the PNJL model as predicted by the OPT (left panel) and the LN approximation (right panel). The LQCD results were obtained in Ref. [66].

4. The entangled Polyakov–Nambu–Jona-Lasinio Model

In chapter 3, the lack of confinement in the NJL model was improved through the implementation of the Polyakov loop. However, another important aspect of QCD, that is not taken into account in the PNJL model, is related to the asymptotic freedom phenomenon. This is a unique characteristic of non-Abelian theories, such as QCD, in which the coupling constant decreases as the energy rises. However, in the effective QCD models considered so far the couplings, G_S and G_V, were taken at constant values. Nevertheless, in order to mimic asymptotic freedom, they should decrease as energy scales, such as the temperature, rise. A way of implementing this behavior was advanced in Ref. [69], where G_S is taken to be an effective vertex, $G_S(\Phi)$, which depends on Φ. This new coupling is called the entanglement vertex, and the interactions are referred to as the entanglement interactions while the PNJL model plus the entanglement vertex is known as entangled PNJL (EPNJL) model.

A possible ansatz for $G_S(\Phi)$, and for $G_V(\Phi)$, is given by [69, 70]

$$G_S(\Phi) = G_S\left[1 - \alpha_1\Phi\bar{\Phi} - \alpha_2\left(\Phi^3 + \bar{\Phi}^3\right)\right], \tag{4.1}$$

$$G_V(\Phi) = G_V\left[1 - \alpha_1\Phi\bar{\Phi} - \alpha_2\left(\Phi^3 + \bar{\Phi}^3\right)\right], \tag{4.2}$$

which preserves chiral symmetry, C symmetry, and extended $Z(3)$ symmetry.

The order parameter $\bar{\sigma}$ is now a function of Φ and $\bar{\Phi}$, and therefore must also be derived with respect to Φ and $\bar{\Phi}$ in the gap equation.

The parameters α_1 and α_2, together with T_0, are fixed in order to reproduce the LQCD data which, at $\mu = 0$, show a coincidence between the pseudocritical temperatures T_Φ and T_σ [71].

Except for the replacements $G_S \to G_S(\Phi)$ and $G_V \to G_V(\Phi)$ the OPT and the LN equations for the PNJL and for the EPNJL models are identical.

4.1. Taylor expansion coefficients

Before evaluating any physical quantities one has to fix the extra parameters α_1 and α_2. Here, following Ref [69] we adopt the values $\alpha_1 = \alpha_2 = 0.2$, which are commonly used in LN evaluations. Note that, if one wants to be rigorous, the parameters α_1 and α_2 should also be fixed within OPT so as to reproduce LQCD data at vanishing density. We leave this exercise, which will have a more quantitative impact, for a future work. For now, it will be sufficient to investigate if the EPNJL thermal couplings will solve the OPT and the LNG_V problem from a qualitative point of view. We found that for the OPT the chiral pseudocritical temperature, T_σ, and the

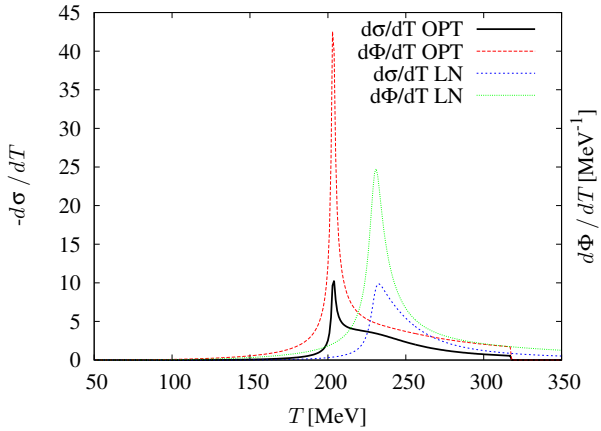

Figure 4.1.: Thermal susceptibilities, $-d\bar{\sigma}/dT$ and $d\Phi/dT$, as functions of the temperature obtained with the OPT and with the LN approximation within the EPNJL model.

pseudocritical temperature for deconfinement, T_Φ, coincide, as can be seen in Fig. 4.1 so that from now on, both transition temperatures will be denoted T_c. It is also important to note that, for the OPT, the crossover region reduces drastically with the inclusion of entanglement.

Figure 4.2 shows the coefficient c_2 obtained with the OPT and with the LN approximation (at $G_V(\Phi) = 0$ and at $G_V(\Phi) = G_S(\Phi)/(N_f N_c)$) for the EPNJL model. For the LNG_V approximation we reproduce the behavior reported in a recent work by Sugano et al. [70]. From a quantitative point of view, it seems that the results for the EPNJL model obtained with the OPT at $T \leq 1.2T_c$ are not so good as those obtained in the PNJL case. However, we are interested in investigating if the c_2 maximum, which appears in the high-T domain ($T > 1.2T_c$), may be at least attenuated by the EPNJL coupling constant which decreases with the temperature. Although the problem is not completely solved one can see, in Fig. 4.2, that the maximum is less pronounced with respect to that seen in the PNJL model. This can also be seen in Figs. 4.3, where the OPT quark number density and the quark number susceptibility are plotted as functions of T/T_c. Therefore, the inclusion of the entanglement give us valuable clues of how the vector repulsive term problem may be solved in the OPT and also in the LN case when $G_V \neq 0$.

At this point it is useful to recall that, in their independent work using the LN approximation with $G_V \neq 0$, Schramm and Steinheimer [59, 68] and also Sugano et al. have faced a similar problem in the evaluation of c_2 and have proposed two different solutions to solve it. Schramm and Steinheimer have suggested that G_V should vanish for $T > T_c$ while Sugano et al. suggest that if one takes $G_V = G_S/3$

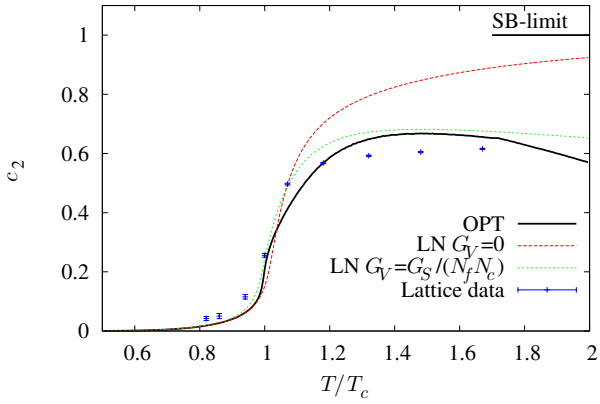

Figure 4.2.: Taylor expansion coefficient, c_2, as a function of T/T_c obtained with the OPT and the LN approximation at $G_V = 0$ and $G_V = 1/(N_f N_c)$ for the EPNJL model. LQCD data from Ref. [66].

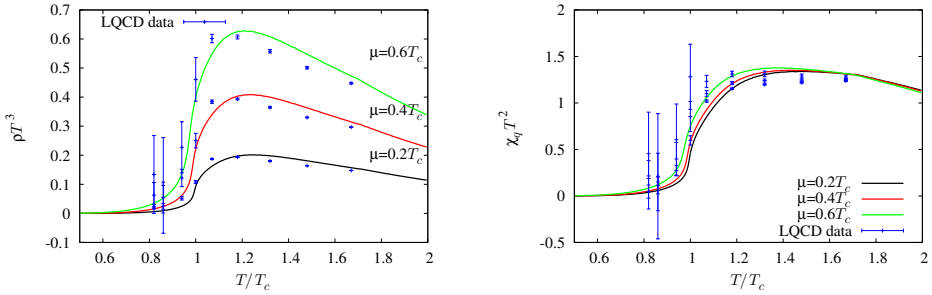

Figure 4.3.: Quark number density, ρ/T^3 (left panel), and quark number susceptibility, χ_q/T^2 (right panel), as functions of T/T_c ($T_c = 203$) MeV for different values of μ obtained with the OPT in the EPNJL model. LQCD data from Ref. [66].

at $T = 0$ and then uses $G_V(\Phi)$ and $G_S(\Phi)$ a reasonable agreement with the lattice results (within eventual error bars) may be achieved for the range $T_c < T < 1.8T_c$. On the other hand, the OPT results suggest that one should pay attention to the thermal behavior of the scalar–pseudoscalar coupling, G_S, which indeed must decrease with T for $T > T_c$. For temperatures lower that $1.1T_c$ this approximation furnishes excellent

numerical results but clearly the running of G_S with T is rather important to describe the susceptibilities in the high-T regime. In order to do that one must find a suitable parametrization for $G(\Phi)$, or alternatively, evaluate higher corrections to the couplings which may turn out to be a cumbersome exercise. A more pragmatic approach would be to describe $G_S(T)$ by means of some QCD inspired ansatz and we are currently investigating all these possibilities.

The main outcome of our investigation is that the two loop OPT corrections, which mimic a repulsive vector channel, produce results equivalent to the LNG_V approximation without the need for an extra parameter.

At temperatures close, or lower than T_c, the OPT results seem to be in better agreement with LQCD than those produced by the traditional approximation (at $G_V = 0$). On the other hand, the OPT (as well as the LNG_V) high-T results indicate that these effective models should be able to mimic asymptotic freedom so that the SB limit is observed.

5. Conclusions

The aim of this work was to improve an alternative non-perturbative analytical method, known as OPT, in order to investigate phase transitions in strongly interacting matter. One motivation is that LQCD is not yet able to probe the regime of highly compressed matter while the traditional LN approximation (or MFA) is notorious for failing in several situations. For example: it violates Landau's theorem for phase transitions in one space dimensions, it is unable to predict the shift on T_c due to the presence of interactions in Bose Einstein condensates and also misses the location of the tricritical point which arises in the phase diagram of planar fermonic systems. In these three situations the OPT, with its finite N_c corrections, has out staged the MFA producing results which are more in line with the lattice data or rigorous phase transition theorems. As far as QCD is concerned this method has been successful in describing chiral symmetry but it had never been used in models which also display confinement. To perform such an application was one of our major goals. Another important remark is that, so far, this method has been used to mainly draw the boundaries of QCD like phase diagrams as well as to evaluate thermodynamical quantities without contrasting the results with available LQCD data, as we have done in this thesis.

We have started our investigation by reviewing, in the framework of the standard NJL model, how the OPT dynamically generates a vector repulsive type of term, which turns out to be similar to that appearing in the LN approximation with $G_V \neq 0$. This term contributes to the pressure at non-vanishing densities only. In contrast, it contributes to the the second cumulant, c_2, due to the non-vanishing derivatives of the vector repulsive term with respect to μ. We have then shown that, as a consequence, the Stefan-Boltzmann limit is not observed. We have also discussed how this vector channel may be explicitly introduced at the classical (tree) level in the original Lagrangian density. Remarking that, this procedure comes with a caveat: the introduction of an extra coupling parameter, G_V. On the other hand, this type of term is naturally generated, via quantum corrections, within the OPT formalism and appears as being proportional to G_S/N_c.

Having identified the problem we have moved to our original piece of work showing how the application of the OPT to the PNJL model brings technical subtleties associated with the evaluation of the traces in color space. To our knowledge this evaluation, for two loop diagrams, has not been done before. We were then able to write down the OPT free energy for the PNJL model including $1/N_c$ suppressed terms. As in the NJL model, we found that, at zero densities, the OPT and the LN approximation did not show significant differences for the thermodynamical quantities analyzed. However, the OPT showed a notorious difference in the interaction

measure with respect to that obtained with the LN approximation (Fig. 3.6) for the PNJL model. At the same time, the cumulant c_2, obtained with the OPT, is in excellent agreement with the LQCD data for $T < 1.1T_c$. At high-T the failure to observe the Stefan-Boltzmann limit showed up in the OPT results which displayed a similar behavior to that observed within the LN approximation when $G_V \neq 0$. We have also observed that, at finite densities, the difference between the order parameters Φ and $\bar{\Phi}$ is in general lower within the OPT than within the LN approximation. Then, in order to improve the OPT behavior at high-T we have considered an entangled type of interaction to analyze the effects produced in the vector term when the NJL coupling constant decreases with the temperature, as in the QCD case. As expected, the entanglement improved the results calculated with the OPT at $T > T_c$ in the EPNJL model. Although a deeper study of the entanglement interaction is needed to produce a more adequate parameter set for the OPT, its inclusion proved the need of enforcing asymptotic freedom within effective models. Another important result is that the crossover region, for both transitions in the EPNJL model was reduced dramatically in the OPT case. This allows us to conclude that, the entanglement interaction affects the pseudocritical temperature as well as the crossover region.

It is important to note that the LN results remained stable at high temperatures for the EPNJL model when $G_V = 0$.

A deeper study of the entanglement interaction for the OPT and the exploration of other possible forms to introduce asymptotic freedom in the PNJL model are some of the most immediate extensions of the present work. Finally, the inclusion of strangeness within the OPT is necessary in order to apply the method to problems related to compact stellar objects.

A. Notation

A.1. Relativistic notation

In this dissertation we have adopted the natural unit system used in modern particle physics, where $c = \hbar = k = 1$, where c is the speed of light, $\hbar$ is the Planck's constant and k represents the Boltzmann constant. Then,

$$[\text{mass}] = [\text{energy}] = [\text{time}]^{-1} = [\text{length}]^{-1} \tag{A.1}$$

In Minkowski space the contravariant position four-vector is denoted by

$$x^\mu = \left(x^0, x^1, x^2, x^3\right) = (t, x, y, z) = (t, \boldsymbol{x}) \,, \tag{A.2}$$

and its covariant form is

$$x^\mu = (x_0, x_1, x_2, x_3) = (t, -x, -y, -z) = (t, -\boldsymbol{x}) \,. \tag{A.3}$$

We employ the following metric

$$g_{\mu\nu} = g^{\mu\nu} = \begin{pmatrix} 1 & 0 & 0 & 0 \\ 0 & -1 & 0 & 0 \\ 0 & 0 & -1 & 0 \\ 0 & 0 & 0 & -1 \end{pmatrix} , \tag{A.4}$$

so that Eq. A.3 may be written as

$$x_\mu = g_{\mu\nu} x^\nu . \tag{A.5}$$

The scalar product of two four-vectors, $a.b$, is defined as

$$a.b = a_\mu b^\mu = g_{\mu\nu} a^\nu b^\mu , \tag{A.6}$$

and is invariant under Lorentz transformations. For this reason, it is called a Lorentz scalar.

A.2. Dirac Matrices

The Dirac matrices are defined by the following anticommutation relation

$$\{\gamma^\mu, \gamma^\nu\} = 2g^{\mu\nu} . \tag{A.7}$$

These mathematical objects can be represented in the standard representation by 4×4 matrices as

$$\gamma^0 = \begin{pmatrix} \mathbf{1}_2 & \mathbf{0}_2 \\ \mathbf{0}_2 & -\mathbf{1}_2 \end{pmatrix}, \quad \gamma^i = \begin{pmatrix} \mathbf{0}_2 & \tau_i \\ -\tau_i & -\mathbf{0}_2 \end{pmatrix}; \quad i = 1, 2, 3. \tag{A.8}$$

where $\mathbf{1}_2$ is the identity matrix 2×2 while τ_i are the Pauli matrices given by

$$\tau_1 = \begin{pmatrix} 0 & 1 \\ 1 & 0 \end{pmatrix}, \quad \tau_2 = \begin{pmatrix} 0 & -i \\ i & 0 \end{pmatrix} \quad \text{and} \quad \tau_3 = \begin{pmatrix} 1 & 0 \\ 0 & -1 \end{pmatrix}. \tag{A.9}$$

The Pauli matrices satisfy the $SU(2)$ algebra

$$[\tau_i, \tau_j] = 2i\epsilon_{ijk}\tau_k, \tag{A.10}$$

where ϵ is the Levi-Civita antisymetric symbol.

The traceless product, γ^5, is given by

$$\gamma^5 = i\gamma^0\gamma^1\gamma^2\gamma^3 = \begin{pmatrix} \mathbf{0} & \mathbf{1}_2 \\ \mathbf{1}_2 & \mathbf{0} \end{pmatrix} \tag{A.11}$$

and satisfies

$$\left\{\gamma^5, \gamma^\mu\right\} = 0. \tag{A.12}$$

B. Matsubara Sums

In this appendix we perform the sum over the Matsubara's frequencies, ω_n, for a system of massive fermions ($m \neq 0$) with a particle-antiparticle asymmetry ($\mu \neq 0$). With this aim let us define a basic function which appears when one evaluates the pressure of a relativistic gas of free fermions. Namely,

$$S = \sum_{n=-\infty}^{\infty} \ln\left[(\omega_n - i\mu)^2 + E_p^2\right], \tag{B.1}$$

where $E_p^2 = \boldsymbol{p}^2 + m^2$ is the dispersion with respect to which S can derived to yield

$$\frac{dS}{dE_p} = \sum_{n=-\infty}^{\infty} \frac{2E_p}{(\omega_n - i\mu)^2 + E_p^2}. \tag{B.2}$$

Remembering that $\omega_n = \frac{2\pi n}{\beta} + \frac{\pi}{\beta}$, let us call $\omega_0 = \frac{\pi}{\beta}$ where $\beta = 1/T$ and $i\mu = z_0$, so that

$$\begin{aligned}
\frac{dS}{dE_p} &= \sum_{n=-\infty}^{\infty} \frac{1}{E_p + i\omega_n - iz_0} + \sum_{n=-\infty}^{\infty} \frac{1}{E_p - i\omega_n + iz_0} \\
&= \sum_{n=-\infty}^{\infty} \frac{1}{E_p + i\omega_0 n + \frac{i\pi}{\beta} - iz_0} + \sum_{n=-\infty}^{\infty} \frac{1}{E_p - i\omega_0 - \frac{i\pi}{\beta} + iz_0} \\
&= \frac{1}{\omega_0}\left[\sum_{n=-\infty}^{\infty} \frac{1}{\frac{E_p}{\omega_0} - \frac{iz_0}{\omega_0} + \frac{i\pi}{\beta\omega_0} + in} + \sum_{n=-\infty}^{\infty} \frac{1}{\frac{E_p}{\omega_0} + \frac{iz_0}{\omega_0} - \frac{i\pi}{\beta\omega_0} - in}\right].
\end{aligned} \tag{B.3}$$

Using the identities

$$\sum_{n=-\infty}^{\infty} \frac{1}{y + in} = \pi \coth \pi y \quad \text{and} \quad \sum_{n=-\infty}^{\infty} \frac{1}{y - in} = \pi \coth \pi y, \tag{B.4}$$

we then obtain

$$\frac{dS}{dE_p} = \frac{\pi}{\omega_0}\left\{\coth\left[\frac{\pi}{\omega_0}\left(E_p - iz_0 + \frac{i\pi}{\beta}\right)\right] + \coth\left[\frac{\pi}{\omega_0}\left(E_p + iz_0 - \frac{i\pi}{\beta}\right)\right]\right\}. \tag{B.5}$$

Now introducing $x_1 = \frac{\pi}{\omega_0}\left(E_p - iz_0 + \frac{i\pi}{\beta}\right)$ and $x_2 = \frac{\pi}{\omega_0}\left(E_p + iz_0 - \frac{i\pi}{\beta}\right)$, such that

$$\begin{aligned}
\frac{dS}{d\left(\pi E_p/\omega_0\right)} &= \coth x_1 + \coth x_2 \\
&= \frac{e^{x_1} + e^{-x_1}}{e^{x_1} - e^{-x_1}} + \frac{e^{x_2} + e^{-x_2}}{e^{x_2} - e^{-x_2}}.
\end{aligned} \tag{B.6}$$

Noting that

$$\frac{d\left(e^{x_1}-e^{-x_1}\right)}{d\left(\pi E_p/\omega_0\right)}=e^{x_1}+e^{-x_1}\quad\text{and}\quad\frac{d\left(e^{x_2}-e^{-x_2}\right)}{d\left(\pi E_p/\omega_0\right)}=e^{x_2}+e^{-x_2}, \tag{B.7}$$

we finally get

$$dS=\int\frac{d\left(e^{x_1}-e^{-x_1}\right)}{e^{x_1}-e^{-x_1}}+\int\frac{d\left(e^{x_2}-e^{-x_2}\right)}{e^{x_2}-e^{-x_2}}, \tag{B.8}$$

and

$$S=\ln\left[e^{x_1}-e^{-x_1}\right]+\ln\left[e^{x_2}-e^{-x_2}\right]. \tag{B.9}$$

Replacing x_1, z_0 and ω_0 yields

$$\begin{aligned}\ln\left[e^{x_1}-e^{-x_1}\right]&=\ln\left[e^{\beta/2\left(E_p+\mu\right)}e^{i\pi/2}-e^{-\beta/2\left(E_p+\mu\right)}e^{-i\pi/2}\right]\\&=\ln\left[\left(e^{\beta/2\left(E_p+\mu\right)}+e^{-\beta/2\left(E_p+\mu\right)}\right)i\sin\pi/2\right]\\&=\ln\left[\left(e^{\beta/2\left(E_p+\mu\right)}+e^{-\beta/2\left(E_p+\mu\right)}\right)\right]-\ln i.\end{aligned} \tag{B.10}$$

Doing the same for $\ln\left[e^{x_2}-e^{-x_2}\right]$ we find S to be

$$\begin{aligned}S&=\ln\left[e^{\beta/2\left(E_p+\mu\right)}+e^{-\beta/2\left(E_p+\mu\right)}\right]+\ln\left[e^{\beta/2\left(E_p-\mu\right)}+e^{-\beta/2\left(E_p-\mu\right)}\right]\\&=\ln\left[1+e^{-\beta\left(E_p+\mu\right)}\right]+\frac{\beta}{2}\left(E_p+\mu\right)+\ln\left[1+e^{-\beta\left(E_p-\mu\right)}\right]+\frac{\beta}{2}\left(E_p-\mu\right).\end{aligned}$$

Then, our starting function can be written as

$$S=\beta E_p+\ln\left[1+e^{-\beta\left(E_p+\mu\right)}\right]+\ln\left[1+e^{-\beta\left(E_p-\mu\right)}\right]. \tag{B.11}$$

Having this equation, which represents a zero point 1PI Green's function at the one loop level, one may easily obtain any n-point Green's function simply by deriving Eq. (B.11) with respect to the mass or the chemical potential. Then, since Eq. (B.11) represents our integral I_1 one sees that I_2 and I_3 may be readily obtained by $I_2\sim\partial I_1/\partial m$ and $I_3\sim\partial I_1/\partial\mu$ as emphasized in the text.

To do that with more rigor, we remark that in Eq. (2.36)

$$\begin{aligned}\sum_{n=-\infty}^{\infty}\ln\left[\left(\omega_n-i\mu\right)^2+E_p^2\right]&=S\\&=\beta E_p+\ln\left[1+e^{-\beta\left(E_p+\mu\right)}\right]+\ln\left[1+e^{-\beta\left(E_p-\mu\right)}\right],\end{aligned} \tag{B.12}$$

which is related to I_1. Then,

$$\sum_{n=-\infty}^{\infty} \frac{1}{(\omega_n - i\mu)^2 + E_p^2} = \frac{1}{2E_p}\frac{\partial S}{\partial E_p}$$
$$= \frac{\beta}{2E_p}\left[1 - \frac{1}{e^{\beta\left(E_p+\mu\right)}+1} - \frac{1}{e^{\beta\left(E_p-\mu\right)}+1}\right], \qquad \text{(B.13)}$$

is related to I_2 while

$$\sum_{n=-\infty}^{\infty} \frac{\omega_n - i\mu}{(\omega_n - i\mu)^2 + E_p^2} = \frac{i}{2}\frac{\partial S}{\partial \mu}$$
$$= \frac{i\beta}{2}\left[\frac{1}{e^{\beta\left(E_p-\mu\right)}+1} - \frac{1}{e^{\beta\left(E_p+\mu\right)}+1}\right], \qquad \text{(B.14)}$$

is related to I_3.

C. Color-trace over two loop contributions

In this Appendix we show how to calculate the color traces that appear in Eq. (3.20). Taking the results from Appendix B let us denote

$$\begin{aligned} S_{ii} &= \sum_{n=-\infty}^{\infty} \ln\left[\left(\omega_n - i\mu'\right)^2 + E_p^2\right] \\ &= \beta E_p + \ln\left[1 + e^{-\beta\left(E_p - \mu'\right)}\right] + \ln\left[1 + e^{-\beta\left(E_p + \mu'\right)}\right], \end{aligned} \tag{C.1}$$

so that S is a diagonal matrix.

Replacing $\mu' = \mu - iA_{ii}$ and $\exp(iA_{ii}) = L_{ii}$ we get

$$S_{ii} = \beta E_p + \ln\left[1 + L_{ii} e^{-\beta\left(E_p - \mu\right)}\right] + \ln\left[1 + L_{ii}^* e^{-\beta\left(E_p + \mu\right)}\right], \tag{C.2}$$

where A_{ii} is the i-th component of the diagonal matrix A_4 and L_{ii} is the i-th component of the matrix L, which can be written in the diagonal form

$$L = \begin{bmatrix} e^{i\theta_1} & 0 & 0 \\ 0 & e^{i\theta_2} & 0 \\ 0 & 0 & e^{-i(\theta_1+\theta_2)} \end{bmatrix}. \tag{C.3}$$

Using the identity $\mathrm{Tr_c} \ln = \ln \det$ we get the the trace of the third term of Eq. (3.20) which represents a one loop contribution

$$\mathrm{Tr_c} S = N_c \beta E_p + \ln\left[g_l^+\left(E_p\right)\right] + \ln\left[g_l^-\left(E_p\right)\right], \tag{C.4}$$

where

$$g_l^+\left(E_p\right) = 1 + 3l e^{-\beta\left(E_p - \mu\right)} + 3l^* e^{-2\beta\left(E_p - \mu\right)} + e^{-3\beta\left(E_p - \mu\right)}, \tag{C.5}$$

$$g_l^-\left(E_p\right) = 1 + 3l^* e^{-\beta\left(E_p + \mu\right)} + 3l e^{-2\beta\left(E_p + \mu\right)} + e^{-3\beta\left(E_p + \mu\right)}. \tag{C.6}$$

The next one loop term is

$$\sum_{n=-\infty}^{\infty} \frac{1}{\left(\omega_n - i\mu'\right)^2 + E_p^2} = \frac{1}{2E_p} \frac{\partial S_{ii}}{\partial E_p}. \tag{C.7}$$

Therefore,

$$\begin{aligned} \mathrm{Tr_c} \sum_{n=-\infty}^{\infty} \frac{1}{\left(\omega_n - i\mu'\right)^2 + E_p^2} &= \frac{1}{2E_p} \frac{\partial \mathrm{Tr_c} S}{\partial E_p} \\ &= \frac{N_c \beta}{2E_p} \left[1 - f_l^+ - f_l^-\right], \end{aligned} \tag{C.8}$$

where the Fermi distributions are given by

$$f_l^+\left(E_p\right)=\frac{le^{-\beta\left(E_p-\mu\right)}+2l^*e^{-2\beta\left(E_p-\mu\right)}+e^{-3\beta\left(E_p-\mu\right)}}{g_l^+\left(E_p\right)}, \tag{C.9}$$

and

$$f_l^-\left(E_p\right)=\frac{l^*e^{-\beta\left(E_p+\mu\right)}+2le^{-2\beta\left(E_p+\mu\right)}+e^{-3\beta\left(E_p+\mu\right)}}{g_l^-\left(E_p\right)}. \tag{C.10}$$

The evaluation of the two loop contributions is more cumbersome as we show next. With the results of appendix B we can write the fifth term of Eq. (3.20) as

$$\sum_{n=-\infty}^{\infty}\frac{\omega_n-i\mu'}{\left(\omega_n-i\mu'\right)^2+E_p^2}\sum_{m=-\infty}^{\infty}\frac{\omega_m-i\mu'}{\left(\omega_m-i\mu'\right)^2+E_q^2}=\frac{i}{2}\frac{\partial S_{ii}\left(E_p\right)}{\partial\mu'}\frac{i}{2}\frac{\partial S_{ii}\left(E_q\right)}{\partial\mu'}, \tag{C.11}$$

and

$$\begin{aligned}\frac{\partial S_{ii}\left(q\right)}{\partial\mu'}\frac{\partial S_{ii}\left(p\right)}{\partial\mu'}=&\beta^2\left[\frac{e^{-\beta\left(E_p-\mu'\right)}}{1+e^{-\beta\left(E_p-\mu'\right)}}-\frac{e^{-\beta\left(E_p+\mu'\right)}}{1+e^{-\beta\left(E_p+\mu'\right)}}\right]\\&\times\left[\frac{e^{-\beta\left(E_q-\mu'\right)}}{1+e^{-\beta\left(E_q-\mu'\right)}}-\frac{e^{-\beta\left(E_q+\mu'\right)}}{1+e^{-\beta\left(E_q+\mu'\right)}}\right]\\=&\beta^2\left[\frac{L_{ii}e^{-\beta\left(E_p-\mu\right)}}{1+L_{ii}e^{-\beta\left(E_p-\mu\right)}}-\frac{L_{ii}^*e^{-\beta\left(E_p+\mu\right)}}{1+L_{ii}^*e^{-\beta\left(E_p+\mu\right)}}\right]\\&\times\left[\frac{L_{ii}e^{-\beta\left(E_q-\mu\right)}}{1+L_{ii}e^{-\beta\left(E_q-\mu\right)}}-\frac{L_{ii}^*e^{-\beta\left(E_q+\mu\right)}}{1+L_{ii}^*e^{-\beta\left(E_q+\mu\right)}}\right]\end{aligned}$$

$$\begin{aligned}\frac{\partial S_{ii}\left(q\right)}{\partial\mu'}\frac{\partial S_{ii}\left(p\right)}{\partial\mu'}=\beta^2\Bigg\{&\frac{L_{ii}^2e^{-\beta\left(E_p-\mu\right)}e^{-\beta\left(E_q-\mu\right)}}{\left[1+L_{ii}e^{-\beta\left(E_p-\mu\right)}\right]\left[1+L_{ii}e^{-\beta\left(E_q-\mu\right)}\right]}\\&-\frac{e^{-\beta\left(E_p-\mu\right)}e^{-\beta\left(E_q+\mu\right)}}{\left[1+L_{ii}e^{-\beta\left(E_p-\mu\right)}\right]\left[1+L_{ii}^*e^{-\beta\left(E_q+\mu\right)}\right]}\\&-\frac{e^{-\beta\left(E_q-\mu\right)}e^{-\beta\left(E_p+\mu\right)}}{\left[1+L_{ii}e^{-\beta\left(E_q-\mu\right)}\right]\left[1+L_{ii}^*e^{-\beta\left(E_p+\mu\right)}\right]}\\&+\frac{L^{*2}_{ii}e^{-\beta\left(E_p+\mu\right)}e^{-\beta\left(E_q+\mu\right)}}{\left[1+L_{ii}^*e^{-\beta\left(E_p+\mu\right)}\right]\left[1+L_{ii}^*e^{-\beta\left(E_q+\mu\right)}\right]}\Bigg\}.\end{aligned} \tag{C.12}$$

After a straightforward but tediously long calculation of each of the four terms appearing in Eq. (C.12) we obtain

$$\begin{aligned}
&\mathrm{Tr_c} \sum_{n=-\infty}^{\infty} \frac{\omega_n - i\mu'}{\left(\omega_n - i\mu'\right)^2 + E_p^2} \sum_{m=-\infty}^{\infty} \frac{\omega_m - i\mu'}{\left(\omega_m - i\mu'\right)^2 + E_q^2} \\
&\quad = -\frac{N_c \beta^2}{4} \left\{ \left[f_l^+ \left(E_p\right) - f_l^- \left(E_p\right) \right] \left[f_l^+ \left(E_q\right) - f_l^- \left(E_q\right) \right] + \Delta_3^2 \right\}, \qquad \text{(C.13)}
\end{aligned}$$

where

$$\begin{aligned}
\Delta_3^2 = &\frac{e^{-\beta\left(E_p-\mu\right)} e^{-\beta\left(E_q-\mu\right)}}{g_l^+(E_p) g_l^+(E_q)} \left\{ 2\left(l^2 - l^*\right) + \left(ll^* - 1\right) \left[e^{-\beta\left(E_p-\mu\right)} + e^{-\beta\left(E_q-\mu\right)} \right] \right. \\
&\left. + 2\left(l^{*2} - l \right) e^{-\beta\left(E_p-\mu\right)} e^{-\beta\left(E_q-\mu\right)} \right\} \\
&- \frac{e^{-\beta\left(E_p-\mu\right)} e^{-\beta\left(E_q+\mu\right)}}{g_l^+(E_p) g_l^-(E_q)} \left\{ 2\left(l - l^{*2} \right) e^{-\beta\left(E_p-\mu\right)} + 2\left(l^* - l^2\right) e^{-\beta\left(E_q+\mu\right)} \right. \\
&\left. + \left(1 - ll^*\right) \left[1 + e^{-\beta\left(E_p-\mu\right)} e^{-\beta\left(E_q+\mu\right)} \right] \right\} \\
&- \frac{e^{-\beta\left(E_q-\mu\right)} e^{-\beta\left(E_p+\mu\right)}}{g_l^+(E_q) g_l^-(E_p)} \left\{ 2\left(l - l^{*2} \right) e^{-\beta\left(E_q-\mu\right)} + 2\left(l^* - l^2\right) e^{-\beta\left(E_p+\mu\right)} \right. \\
&\left. + \left(1 - ll^*\right) \left[1 + e^{-\beta\left(E_q-\mu\right)} e^{-\beta\left(E_p+\mu\right)} \right] \right\} \\
&+ \frac{e^{-\beta\left(E_p+\mu\right)} e^{-\beta\left(E_q+\mu\right)}}{g_l^-(E_p) g_l^-(E_q)} \left\{ 2\left(l^{*2} - l \right) + \left(ll^* - 1\right) \left[e^{-\beta\left(E_p+\mu\right)} + e^{-\beta\left(E_q+\mu\right)} \right] \right. \\
&\left. + 2\left(l^2 - l^*\right) e^{-\beta\left(E_p+\mu\right)} e^{-\beta\left(E_q+\mu\right)} \right\}. \qquad \text{(C.14)}
\end{aligned}$$

Finally, for the last term of Eq. (3.20) we have

$$\sum_{n=-\infty}^{\infty} \frac{1}{\left(\omega_n - i\mu'\right)^2 + E_p^2} \sum_{m=-\infty}^{\infty} \frac{1}{\left(\omega_m - i\mu'\right)^2 + E_q^2} = \frac{1}{2E_p} \frac{\partial S_{ii}\left(E_p\right)}{\partial E_p} \frac{1}{2E_q} \frac{\partial S_{ii}\left(E_q\right)}{\partial E_q}. \qquad \text{(C.15)}$$

Then,

$$\begin{aligned}\frac{\partial S_{ii}\left(E_p\right)}{\partial E_p}\frac{\partial S_{ii}\left(E_q\right)}{\partial E_q} =&\beta^2\left[1-\frac{e^{-\beta\left(E_p-\mu'\right)}}{1+e^{-\beta\left(E_p-\mu'\right)}}-\frac{e^{-\beta\left(E_p+\mu'\right)}}{1+e^{-\beta\left(E_p+\mu'\right)}}\right]\\ &\times\left[1-\frac{e^{-\beta\left(E_q-\mu'\right)}}{1+e^{-\beta\left(E_q-\mu'\right)}}-\frac{e^{-\beta\left(E_q+\mu'\right)}}{1+e^{-\beta\left(E_q+\mu'\right)}}\right]\\ =&\beta^2\left[1-\frac{L_{ii}e^{-\beta\left(E_p-\mu\right)}}{1+L_{ii}e^{-\beta\left(E_p-\mu\right)}}-\frac{L_{ii}^*e^{-\beta\left(E_p+\mu\right)}}{1+L_{ii}^*e^{-\beta\left(E_p+\mu\right)}}\right]\\ &\times\left[1-\frac{L_{ii}e^{-\beta\left(E_q-\mu\right)}}{1+L_{ii}e^{-\beta\left(E_q-\mu\right)}}-\frac{L_{ii}^*e^{-\beta\left(E_q+\mu\right)}}{1+L_{ii}^*e^{-\beta\left(E_q+\mu\right)}}\right]. \qquad \text{(C.16)}\end{aligned}$$

Finally, the remaining trace gives

$$\begin{aligned}&\mathrm{Tr_c}\sum_{n=-\infty}^{\infty}\frac{1}{\left(\omega_n-i\mu'\right)^2+E_p^2}\sum_{m=-\infty}^{\infty}\frac{1}{\left(\omega_m-i\mu'\right)^2+E_q^2}\\ &\quad=\frac{N_c\beta^2}{4E_pE_q}\left\{\left[1-f_l^+\left(E_p\right)-f_l^-\left(E_p\right)\right]\left[1-f_l^+\left(E_q\right)-f_l^-\left(E_q\right)\right]+\Delta_2^2\right\}, \qquad \text{(C.17)}\end{aligned}$$

where

$$\begin{aligned}\Delta_2^2=&\frac{e^{-\beta\left(E_p-\mu\right)}e^{-\beta\left(E_q-\mu\right)}}{g_l^+(E_p)g_l^+(E_q)}\left\{2\left(l^2-l^*\right)+\left(ll^*-1\right)\left[e^{-\beta\left(E_p-\mu\right)}+e^{-\beta\left(E_q-\mu\right)}\right]\right.\\ &\left.+2\left(l^{*2}-l\right)e^{-\beta\left(E_p-\mu\right)}e^{-\beta\left(E_q-\mu\right)}\right\}\\ &+\frac{e^{-\beta\left(E_p-\mu\right)}e^{-\beta\left(E_q+\mu\right)}}{g_l^+(E_p)g_l^-(E_q)}\left\{2\left(l-l^{*2}\right)e^{-\beta\left(E_p-\mu\right)}+2\left(l^*-l^2\right)e^{-\beta\left(E_q+\mu\right)}\right.\\ &\left.+\left(1-ll^*\right)\left[1+e^{-\beta\left(E_p-\mu\right)}e^{-\beta\left(E_q+\mu\right)}\right]\right\}\\ &+\frac{e^{-\beta\left(E_q-\mu\right)}e^{-\beta\left(E_p+\mu\right)}}{g_l^+(E_q)g_l^-(E_p)}\left\{2\left(l-l^{*2}\right)e^{-\beta\left(E_q-\mu\right)}+2\left(l^*-l^2\right)e^{-\beta\left(E_p+\mu\right)}\right.\\ &\left.+\left(1-ll^*\right)\left[1+e^{-\beta\left(E_q-\mu\right)}e^{-\beta\left(E_p+\mu\right)}\right]\right\}\\ &+\frac{e^{-\beta\left(E_p+\mu\right)}e^{-\beta\left(E_q+\mu\right)}}{g_l^-(E_p)g_l^-(E_q)}\left\{2\left(l^{*2}-l\right)+\left(ll^*-1\right)\left[e^{-\beta\left(E_p+\mu\right)}+e^{-\beta\left(E_q+\mu\right)}\right]\right.\\ &\left.+2\left(l^2-l^*\right)e^{-\beta\left(E_p+\mu\right)}e^{-\beta\left(E_q+\mu\right)}\right\}. \qquad \text{(C.18)}\end{aligned}$$

Bibliography

[1] J. C. Collins and M. J. Perry. Superdense matter: Neutrons or asymptotically free quarks? *Phys. Rev. Lett.*, 34:1353–1356, May 1975.

[2] Michael Buballa. Njl-model analysis of dense quark matter. *Phys.Rept.*, 407:205–376, 2005.

[3] Y. Nambu and G. Jona-Lasinio. Dynamical model of elementary particles based on an analogy with superconductivity. i. *Phys. Rev.*, 122:345–358, Apr 1961.

[4] Y. Nambu and G. Jona-Lasinio. Dynamical model of elementary particles based on an analogy with superconductivity. ii. *Phys. Rev.*, 124:246–254, Oct 1961.

[5] Peter N. Meisinger and Michael C. Ogilvie. Coupling the deconfining and chiral transitions. *Nucl. Phys B - Proc. Supp.*, 47(1–3):519 – 522, 1996.

[6] Luca Bonanno and Armen Sedrakian. Composition and stability of hybrid stars with hyperons and quark color-superconductivity. *A&A*, 539:A16, 2012.

[7] C. H. Lenzi and G. Lugones. Hybrid stars in the light of the massive pulsar psr j1614–2230. *ApJ*, 759(1):57, 2012.

[8] Domenico Logoteta, Constança Providência, and Isaac Vidaña. Formation of hybrid stars from metastable hadronic stars. *Phys. Rev. C*, 88:055802, Nov 2013.

[9] G. Y. Shao, M. Colonna, M. Di Toro, Y. X. Liu, and B. Liu. Isoscalar-vector interaction and hybrid quark core in massive neutron stars. *Phys. Rev. D*, 87:096012, May 2013.

[10] Takahiro Sasaki, Nobutoshi Yasutake, Michio Kohno, Hiroaki Kouno, and Masanobu Yahiro. Determination of quark-hadron transition from lattice QCD and neutron-star observation.

[11] Kota Masuda, Tetsuo Hatsuda, and Tatsuyuki Takatsuka. Hadron–quark crossover and massive hybrid stars. *PTEP*, 2013(7), 2013.

[12] B.D.Serot and J.D. Walecka. *Advances in Nuclear Physics*, volume 16. Plenum, New York, 1986.

[13] Volker Koch, Tamas S. Biro, Jutta Kunz, and Ulrich Mosel. A chirally invariant fermionic field theory for nuclear matter. *Phys.Lett. B*, 185(1–2):1 – 5, 1987.

[14] Débora P. Menezes, Marcus B. Pinto, Luis B. Castro, Pedro Costa, and Constança Providência. Repulsive vector interaction in three-flavor magnetized quark and stellar matter. *Phys. Rev. C*, 89:055207, May 2014.

[15] Robson Z. Denke and Marcus Benghi Pinto. Influence of a repulsive vector coupling in magnetized quark matter. *Phys. Rev. D*, 88:056008, Sep 2013.

[16] Demorest P. B., Pennucci T., Ransom S. M., Roberts M. S. E., and Hessels J. W. T. A two-solar-mass neutron star measured using Shapiro delay. *Nature*, 467(7319):1081–1083, oct 2010. 10.1038/nature09466.

[17] John Antoniadis, Paulo C. C. Freire, Norbert Wex, Thomas M. Tauris, Ryan S. Lynch, Marten H. van Kerkwijk, Michael Kramer, Cees Bassa, Vik S. Dhillon, Thomas Driebe, Jason W. T. Hessels, Victoria M. Kaspi, Vladislav I. Kondratiev, Norbert Langer, Thomas R. Marsh, Maura A. McLaughlin, Timothy T. Pennucci, Scott M. Ransom, Ingrid H. Stairs, Joeri van Leeuwen, Joris P. W. Verbiest, and David G. Whelan. A massive pulsar in a compact relativistic binary. *Science*, 340(6131), 2013.

[18] J. B. Kogut and C. G. Strouthos. Chiral symmetry restoration in the three-dimensional four-fermion model at nonzero temperature and density. *Phys. Rev. D*, 63:054502, Jan 2001.

[19] Philippe de Forcrand and Owe Philipsen. The chiral critical point of n f = 3 qcd at finite density to the order $(\mu/t)^4$. *JHEP*, 2008(11):012, 2008.

[20] Kenji Fukushima. Critical surface in hot and dense qcd with the vector interaction. *Phys. Rev. D*, 78:114019, Dec 2008.

[21] Benjamin Svetitsky and Laurence G. Yaffe. Critical behavior at finite-temperature confinement transitions. *Nucl.Phys. B*, 210(4):423 – 447, 1982.

[22] Robert D. Pisarski and Frank Wilczek. Remarks on the chiral phase transition in chromodynamics. *Phys. Rev. D*, 29:338–341, Jan 1984.

[23] Aoki Y., Endrodi G., Fodor Z., Katz S. D., and Szabo K. K. The order of the quantum chromodynamics transition predicted by the standard model of particle physics. *Nature*, 443(7112):675–678, oct 2006. 10.1038/nature05120.

[24] Kenji Fukushima and Tetsuo Hatsuda. The phase diagram of dense QCD. *Rept.Prog.Phys.*, 74:014001, 2011.

[25] Owe Philipsen. Lattice QCD at non-zero temperature and baryon density.

[26] C.R. Allton, S. Ejiri, S.J. Hands, O. Kaczmarek, F. Karsch, E. Laermann, and Ch. Schmidt. {QCD} at non-zero temperature and density from the lattice. *Nucl.Phys B - Proc. Supp.*, 141(0):186 – 190, 2005. {QCD} Down Under Proceedings of the Workshop on Quantum Chromodynamics Wokshop on Quantum Chromodynamics.

[27] Gert Aarts. Developments in lattice QCD for matter at high temperature and density.

[28] Adrian Dumitru, Robert D. Pisarski, and Detlef Zschiesche. Dense quarks, and the fermion sign problem, in a su(n) matrix model. *Phys. Rev. D*, 72:065008, Sep 2005.

[29] Paolo Finelli. Chiral symmetry. University Lecture, 2012.

[30] Thiago Carvalho Peixoto. Dinânica das transições quiral e de desconfinamento da cromodinâmica quântica como o modelo polyakov-nambu-jona-lasinio. Master's thesis, UNESP, 2014.

[31] Topi Kähärä. *Thermodynamics of Two-Flavor QCD from Chiral Models with Polyakov Loop*. PhD thesis, University of Jyväskylä, 2010.

[32] Kenji Fukushima and Chihiro Sasaki. The phase diagram of nuclear and quark matter at high baryon density. *Prog.Part.Nucl.Phys*, 72(0):99 – 154, 2013.

[33] Tetsuo Hatsuda and Teiji Kunihiro. QCD phenomenology based on a chiral effective Lagrangian. *Phys.Rept.*, 247:221–367, 1994.

[34] David Bailin and Alexander Love. *Introduction to Gauge Field Theory*. Taylor & Francis Group, 1993.

[35] Joseph I. Kapusta. *Finite-temperature field theory*. Cambridge University Press, 1989.

[36] Sidney Coleman. *Aspects of Symmetry*. Cambridge University Press, 1985.

[37] Sunil K. Gandhi, H.F. Jones, and Marcus B. Pinto. The δ-expansion in the large-n limit. *Nucl. Phys. B*, 359(2–3):429 – 440, 1991.

[38] Sunil K. Gandhi and Marcus B. Pinto. δ expansion of models with chiral-symmetry breaking. *Phys. Rev. D*, 46:2570–2577, Sep 1992.

[39] G. Krein, R.S. Marques de Carvalho, D.P. Menezes, Marina Nielsen, and M.B. Pinto. Optimized delta expansion for relativistic nuclear models. *Eur.Phys.J.*, A1:45–53, 1998.

[40] P. M. Stevenson. Optimized perturbation theory. *Phys. Rev. D*, 23:2916–2944, Jun 1981.

[41] I. R. C. Buckley, A. Duncan, and H. F. Jones. Proof of the convergence of the linear δ expansion: Zero dimensions. *Phys. Rev. D*, 47:2554–2559, Mar 1993.

[42] Frederico F. de Souza Cruz, Marcus B. Pinto, and Rudnei O. Ramos. Transition temperature for weakly interacting homogeneous bose gases. *Phys. Rev. B*, 64:014515, Jun 2001.

[43] Jean-Loïc Kneur, André Neveu, and Marcus B. Pinto. Improved optimization of perturbation theory: Applications to the oscillator energy levels and bose-einstein condensate critical temperature. *Phys. Rev. A*, 69:053624, May 2004.

[44] Heron Caldas, Jean-Lo¨ ic Kneur, Marcus Benghi Pinto, and Rudnei O. Ramos. Critical dopant concentration in polyacetylene and phase diagram from a continuous four-fermi model. *Phys. Rev. B*, 77:205109, May 2008.

[45] Jens O. Andersen, Lars E. Leganger, Michael Strickland, and Nan Su. Three-loop HTL QCD thermodynamics. *JHEP*, 1108:053, 2011.

[46] Jean-Loïc Kneur and André Neveu. Renormalization group improved optimized perturbation theory: Revisiting the mass gap of the $o(2n)$ gross-neveu model. *Phys. Rev. D*, 81:125012, Jun 2010.

[47] Jean-Loïc Kneur and André Neveu. $\Lambda_{\overline{\rm ms}}^{\rm qcd}$ from renormalization group optimized perturbation. *Phys. Rev. D*, 85:014005, Jan 2012.

[48] Jean-Loïc Kneur and André Neveu. α_S from f_π and renormalization group optimized perturbation theory. *Phys. Rev. D*, 88:074025, Oct 2013.

[49] Jean-Loïc Kneur, Marcus Benghi Pinto, and Rudnei O. Ramos. Thermodynamics and phase structure of the two-flavor nambu–jona-lasinio model beyond large nc. *Phys. Rev. C*, 81:065205, Jun 2010.

[50] Ederson Staudt. *Teorias Fermiônicas Efetivas Sob Condições Extremas.* PhD thesis, UNIVERSIDADE FEDERAL DE SANTA CATARINA, 2009.

[51] L. Dolan and R. Jackiw. Symmetry behavior at finite temperature. *Phys. Rev. D*, 9:3320–3341, Jun 1974.

[52] Tormond Gjestland. Gauge theories at finite temperature. Master's thesis, NTNU, 2007.

[53] Murray Gell-Mann, R. J. Oakes, and B. Renner. Behavior of current divergences under $\mathrm{su}_3 \times \mathrm{su}_3$. *Phys. Rev.*, 175:2195–2199, Nov 1968.

[54] Simon Hands. The Phase diagram of QCD. *Contemp.Phys.*, 42:209–225, 2001.

[55] Mingmei Xu and Yuanfang Wu. Inflection point as a characteristic of the QCD critical point. *Nucl. Phys. A*, 927:69–77, 2014.

[56] M. Bluhm, P. Alba, W. Alberico, R. Bellwied, V. Mantovani Sarti, M. Nahrgang, and C. Ratti. Determination of freeze-out conditions from fluctuation observables measured at {RHIC}. *Nucl. Phys. A*, (0):–, 2014.

[57] Sanjay K. Ghosh, Tamal K. Mukherjee, Munshi G. Mustafa, and Rajarshi Ray. Susceptibilities and speed of sound from the polyakov-nambu-jona-lasinio model. *Phys. Rev. D*, 73:114007, Jun 2006.

[58] Najmul Haque, Munshi G. Mustafa, and Michael Strickland. Two-loop hard thermal loop pressure at finite temperature and chemical potential. *Phys. Rev. D*, 87:105007, May 2013.

[59] J. Steinheimer and S. Schramm. The problem of repulsive quark interactions – lattice versus mean field models. *Phys. Lett. B*, 696(3):257 – 261, 2011.

[60] Murray Gell-Mann. Symmetries of baryons and mesons. *Phys. Rev.*, 125:1067–1084, Feb 1962.

[61] H. Hansen, W. M. Alberico, A. Beraudo, A. Molinari, M. Nardi, and C. Ratti. Mesonic correlation functions at finite temperature and density in the nambu–jona-lasinio model with a polyakov loop. *Phys. Rev. D*, 75:065004, Mar 2007.

[62] C. Ratti, S. Rößner, M.A. Thaler, and W. Weise. Thermodynamics of the pnjl model. *Eur.Phys.J. C*, 49(1):213–217, 2007.

[63] Kenji Fukushima. Chiral effective model with the polyakov loop. *Phys. Lett. B*, 591(3–4):277 – 284, 2004.

[64] Claudia Ratti, Michael A. Thaler, and Wolfram Weise. Phases of qcd: Lattice thermodynamics and a field theoretical model. *Phys. Rev. D*, 73:014019, Jan 2006.

[65] J Greensite. The confinement problem in lattice gauge theory. *Prog.Part.Nucl.Phys*, 51(1):1 – 83, 2003.

[66] S. Ejiri, Y. Maezawa, N. Ukita, S. Aoki, T. Hatsuda, N. Ishii, K. Kanaya, and T. Umeda. Equation of state and heavy-quark free energy at finite temperature and density in two flavor lattice qcd with wilson quark action. *Phys. Rev. D*, 82:014508, Jul 2010.

[67] Yuji Sakai, Kouji Kashiwa, Hiroaki Kouno, Masayuki Matsuzaki, and Masanobu Yahiro. Determination of qcd phase diagram from the imaginary chemical potential region. *Phys. Rev. D*, 79:096001, May 2009.

[68] Jan Steinheimer and Stefan Schramm. Do lattice data constrain the vector interaction strength of qcd? *Phys. Lett. B*, 736(0):241 – 245, 2014.

[69] Yuji Sakai, Takahiro Sasaki, Hiroaki Kouno, and Masanobu Yahiro. Entanglement between deconfinement transition and chiral symmetry restoration. *Phys. Rev. D*, 82:076003, Oct 2010.

[70] Junpei Sugano, Junichi Takahashi, Masahiro Ishii, Hiroaki Kouno, and Masanobu Yahiro. Determination of the strength of the vector-type four-quark interaction in the entanglement polyakov-loop extended nambu–jona-lasinio model. *Phys. Rev. D*, 90:037901, Aug 2014.

[71] Frithjof Karsch and Edwin Laermann. Susceptibilities, the specific heat, and a cumulant in two-flavor qcd. *Phys. Rev. D*, 50:6954–6962, Dec 1994.